# Laser-Driven Multi-GeV Muon Sources: Production and Applications

A. Cimmino[1], R. Versaci[1], A. Balaceanu[2], F. Bossi[3], S.V. Bulanov[1], L. Calvin[4], L. Chen[5], C. Daponta[6], T. Ditmire[7], M. Dobre[2], D. Doria[2], S. Eliezer[8], A. Erlandson[9], K. Fleck[4], T. Foster[4], E. Gerstmayr[4], P. Ghenuche[2], Y. Gu[10], Z. Henis[8], H. Maguire[4], D. Margarone[1], B. Miao[11], S.D. Moustaizis[6], M. Nevrkla[1], I. Ploumistakis[6], B. Reagan[12,13], E. Rockafellow[14], B. Rus[1], A. Saftoiu[2], G. Sarri[4], J.E. Shrock[14], J. Sisma[1,15], D. Terzani[16], M. Tytgat[17], P. Valenta[1], C. Vancea[2], W. Wang[18], J. Williams[13], F. Zhang[19], F. Zhou[19], and G.M. Grittani[1]

[1]*ELI Beamlines Facility, The Extreme Light Infrastructure ERIC, Za Radnicí 835, 252 41 Dolní Břežany, CZ*
[2]*IFIN-HH, Extreme Light Infrastructure-Nuclear Physics, Str. Reactorului no.30, P.O. box MG-6, 077125 Magurele, RO*
[3]*INFN, Laboratori Nazionali di Frascati, Via Enrico Fermi 54, 00044 Frascati (RM), IT*
[4]*School of Mathematics and Physics, Queen's University Belfast, BT7 1NN, Belfast, UK*
[5]*Institute of Modern Physics, Chinese Academy of Science, Lanzhou 730000, CN*
[6]*Technical University of Crete, Lab of Matter Structure and Laser Physics, Chania, Crete, GR*
[7]*Dep. of Physics, The University of Texas at Austin, 2515 Speedway, C1600, Austin, TX 78712-1192, USA*
[8]*Applied Physics, Soreq Nuclear Research Center, Yavne, IL*
[9]*Canadian Nuclear Laboratories, Chalk River Lab., 286 Plant Rd, Chalk River, ON K0J 1J0, CA*
[10]*Shanghai Institute of Laser Plasma, China Academy of Engineering Physics, Shanghai 201800, CN*
[11]*Department of Physics, University of Maryland, College Park, MD 20742, USA*
[12]*Lawrence Livermore National Laboratory, Livermore, CA 94550, USA*
[13]*Dep. of Electrical and Computer Engineering, Colorado State University, Fort Collins, CO, 80523, USA*
[14]*Institute for Research in Electronics and Applied Physics and Department of Physics, University of Maryland, College Park, MD, 20742, USA*
[15]*Faculty of Nuclear Sciences and Physical Engineering, ČVUT, Břehová 7, 11519 Prague, CZ*
[16]*Berkeley Lab Laser Accelerator Center, Lawrence Berkeley National Laboratory, 1 Cyclotron Road, Berkeley, CA 94720, USA*
[17]*Inter-University Institute for High Energies, Vrije Universiteit Brussel, 1050 Brussels, BE*
[18]*State Key Laboratory of High Field Laser Physics and CAS Center for Excellence in Ultra-intense Laser Science, Shanghai Institute of Optics and Fine Mechanics CAS, Shanghai 201800, CN*
[19]*National Key Laboratory of Plasma Physics, Laser Fusion Research Center, Academy of Engineering Physics, Mianyang 621900, CN*

**Abstract**

Recent advances in laser wakefield acceleration (LWFA) provide a route to generate multi-GeV electron beams, enabling transportable, laser-driven muon sources. By directing the electron bunches onto high-Z targets, muons are produced through Bethe–Heitler pair creation and pion decay processes. The resulting pulsed flux can exceed the natural cosmic background while offering tunable energy and directionality. This work reviews the current status of laser-driven muon sources, scaling laws, experimental demonstrations at leading facilities, and detection techniques. Reported LWFA experiments have observed directed, high-energy and lower-energy, isotropic muon emissions. Measured muon lifetimes matched the well-known value, providing evidence of muon generation. We discuss performance projections for next-generation high-repetition-rate systems capable of substantially enhanced muon flux. Such compact sources open new opportunities for muon-radiography, nuclear security, high-energy physics research, and exploratory concepts such as muon-catalyzed fusion. Continued development of LWFA electron drivers and detector systems is critical to realizing these applications.

**Keywords:** laser wakefield acceleration; muon beams; Bethe–Heitler process; chirped pulse amplification; petawatt lasers.

This peer-reviewed article has been accepted for publication but not yet copyedited or typeset, and so may be subject to change during the production process. The article is considered published and may be cited using its DOI.
This is an Open Access article, distributed under the terms of the Creative Commons Attribution licence (https://creativecommons.org/licenses/by/4.0/), which permits unrestricted re-use, distribution, and reproduction in any medium, provided the original work is properly cited.

10.1017/hpl.2026.10210
Downloaded from https://www.cambridge.org/core. 19 Nov 2026 at 10:23:14, subject to the Cambridge Core terms of use.

## 1. Introduction

Since their discovery[1] in 1936 by Neddermeyer and Anderson, muons have occupied a position of central importance in the field of fundamental physics, where they have served as probes for testing theories and understanding particle interactions[2,3]. In addition, because of their exceptional penetration power and non-destructive properties, muons have found a broad range of applications in imaging large or dense objects, enabling the investigation of otherwise inaccessible structures and materials[4].

In nature, muons are predominantly produced as secondary particles arising from the interactions of high-energy cosmic rays with atomic nuclei in the Earth's atmosphere. These processes yield a nearly constant flux of atmospheric muons, reaching the Earth's surface. The intrinsically limited flux of cosmic ray muons (with an average flux of about 1 muon/cm$^2$/minute and a mean energy of $\sim$4 GeV at sea level)[5], combined with the lack of inherent directionality of such naturally occurring muons, has motivated the pursuit of artificial sources. These are most commonly realized through the collisions of proton beams with low-Z targets, such as graphite or beryllium[6], where the ensuing photo-nuclear interactions yield muon beams with typical energies extending to several tens of MeV[7–10], reaching into the hundreds of GeV at dedicated high-particle-energy installations such as CERN[11,12]. An alternative route to muon generation is through the interaction of GeV-scale electron beams with high-Z targets, such as tungsten[13,14], producing muons via Bethe–Heitler (BH) pair creation and via pion photo- or electro-production ($\pi$P) and decay[15]. However, to reach multi-GeV energies, conventional radio-frequency (RF) electron accelerators need to be large (typical acceleration gradients of the order of 10 MV/m)[16]. Additionally, leptonic machines suffer synchrotron power losses while linacs experience breakdown in RF cavities[16,17].

Recent developments in laser-plasma interaction physics have opened a potential routes toward more compact electron-produced muon beams sources. Demonstration of multi-GeV electron beams generated by laser wakefield acceleration (LWFA) in facilities occupying only a few tens of square meters[18–21] shows a possible path toward the realization of compact muon sources. This development suggests that transportable multi-GeV electron accelerators may become feasible, potentially reaching energies up to 100 GeV[22]. Such systems could broaden the scientific and technological applications of high-energy muon beams. Several experimental groups have recently reported observations of muon production using laser-accelerated electrons[23–26]. These results support the feasibility of the approach and motivate further optimization. This breakthrough further suggests the possibility of developing potentially transportable multi-GeV electron accelerators (up to 100 GeV [22]), which could broaden the scientific and technological applications of high-energy muon beams. Recently, several experimental groups have reported direct observations of muon production using laser-accelerated electrons [23–26], supporting the viability of this approach and motivating continued efforts to refine and optimize it.

This paper provides a comprehensive review of the state of the art and outlines future directions for research in the field.

Correspondence to: Email: anna.cimmino@eli-beams.eu - Correspondence to: Email: roberto.versaci@eli-beams.eu - Correspondence to: Email: gabrielemaria.grittani@eli-beams.eu

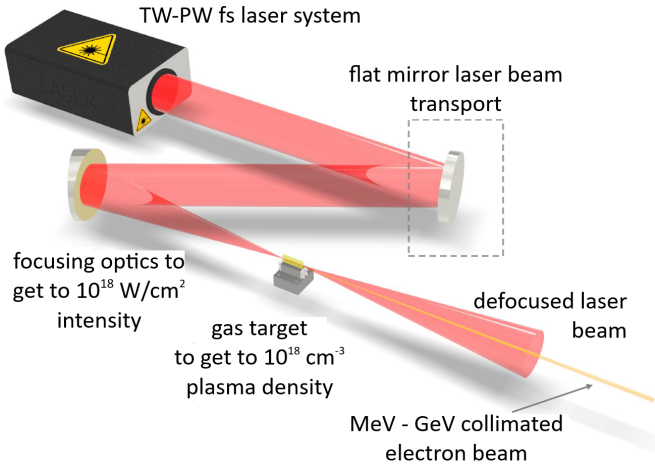



**Figure 1.** Simplified scheme of LWFA. High power ultra-short laser pulses are transported by flat mirrors to a reflective optical element that focuses the light down to 10s $\mu$m focal spot. The interaction of the focused laser pulse with a gas jet creates an underdense plasma, where the electron beam can be accelerated in the plasma waves formed.

## 2. Multi-GeV electrons from LWFA

Laser Wakefield Acceleration (LWFA) was first proposed in a theoretical paper in 1979[27]. At that time, however, laser systems with sufficient power to realize experimentally the concept were not yet available. The invention of Chirped Pulse Amplification (CPA) in 1985[28] marked a decisive advancement, as it dramatically increased the maximum laser peak power and focused intensity attainable. CPA technology enabled the first experimental demonstrations, in 2004, of quasi-monoenergetic (QME) electron beams produced by LWFA[29–31]. Among currently available approaches, LWFA represents the most compact and cost effective method for generating multi-GeV electron beams. GeV-electron acceleration can be produced in plasmas under 10 cm in length, driven by ultra-fast CPA lasers with footprints of only $\sim$10-30 m$^2$. The basic principle is shown in Figure 1. An ultra-short (fs) high-power (>TW) laser pulse is focused by a (usually reflective) focusing optic into a gas target, where plasma waves and electric fields (wakefields) are excited. These fields can exceed those achievable with conventional RF accelerator technology by three to four orders of magnitude[27,32] since con-



Downloaded from https://www.cambridge.org/core. 19 Nov 2026 at 10:23:14, subject to the Cambridge Core terms of use.

ventional accelerators are hindered by material breakdown. The electron energy depends on several factors, including laser pulse amplitude and duration, plasma target density, and whether the laser pulse propagates inside a preformed plasma channel. The quality of the accelerated electron beam, defined by its longitudinal and transverse emittance, depends on how electrons are injected into the accelerating phase of the plasma wave. Different injection schemes, such as the self-injection mechanism proposed in Bulanov *et al.*[33], ionization-induced injection[34,35], colliding-pulse injection[36], or down-ramp density injection[37] govern how electrons enter the accelerating phase of the wakefield, thereby shaping the beam's emittance. Precise control of the injection process is essential for producing high quality, tunable electron beams suitable for applications like radiation sources and secondary particle generation, such as muon beams.

While the physical mechanisms governing muon production from high-energy electrons interacting with dense targets are well established[38], the generation of laser-plasma-accelerated electron beams with the energy, charge, stability and phase-space characteristics required for reproducible muon production remains an active area of research. Continued advances in scaling laws and experimental optimization are therefore essential to fully exploit laser-driven muon sources. Sections 2.1 and 2.2 provide more details on scaling laws essential for evaluating the performance of laser-driven muon sources and experimental demonstrations of multi-GeV electron beams.

### *2.1. Scaling laws for multi-GeV LWFA electrons*

Scaling laws for multi-GeV LWFA electrons are based on the relationship between laser properties (e.g. wavelength, power) and plasma properties (e.g. density). While the underlying physics of has been reviewed extensively elsewhere[39–42], relevant scaling relations are summarized here. Numerical coefficients approximately equal to unity are omitted for clarity and to illustrate the fundamental physics. In the original Tajima-Dawson model[27], the maximum electron energy is

$$\varepsilon_m = 2m_e c^2 \gamma_{ph}^2 \tag{1}$$

where $m_e$ is the electron mass, $c$ is the speed of light, and $\gamma_{ph}$ is the Lorentz factor associated with the phase velocity of the wake wave. For an electromagnetic wave propagating in a collisionless plasma, $\gamma_{ph} \simeq \omega_0/\omega_{pe} = (n_{cr}/n_e)^{1/2}$, where $\omega_0$ is the laser pulse waist, $\omega_{pe} = (4\pi n_e e^2/m_e)^{1/2}$ is the plasma frequency, $n_e$ is the electron plasma density, and $n_{cr} = m_e\omega_0^2/(4\pi e^2)$ is the critical density. Eq. 1 assumes that the normalized amplitude of the driver laser pulse, $a_0$, is close to unity. Simulations from Valenta *et al.*[41] suggest $a_0 \sim 2.5$ is favorable for maximizing electron energy. This scaling shows that lower plasma density allows higher electron energy. However, in practice the acceleration length, guiding conditions, laser depletion, and beam loading also impose constraints.

A laser pulse with a finite focal waist generates a plasma-wakefield structure in what is commonly described as the *blowout regime* producing a plasma cavity, or *bubble*[43]. All electrons in the path of the laser are expelled outward, driving electron flow around the bubble in the collisionless plasma. The interior of the cavity is left positively charged, which attracts electrons from the surrounding regions that were not directly affected by the ponderomotive force. At equilibrium the pondermotive potential in the cavity is equal to the electrostatic potential and the transverse size of this cavity is given by $r_\omega \approx c\sqrt{a_0}/\omega_{pe}$. This assumes self-focusing which results in the laser pulse channeling inside a finite radius channel, aiding in the bubble formation and propagation. Self-focusing occurs when $P/\bar{P} > \gamma_{ph}^2$, where $P$ is the laser power and $\bar{P} = 2m_e^2c^5/e^2$ is the critical power in the theory of relativistic self-focusing[44]. As the laser pulse propagates in the plasma, its amplitude and waist change but its power is assumes constant. Consequently the relationship between the electromagnetic wave amplitude and power $P$ is,

$$a_0^3 = \frac{P}{\bar{P}}\gamma_{ph}^2 \tag{2}$$

and the corresponding acceleration length is given by

$$l_{acc} \approx \lambda_0\left(\frac{P}{\bar{P}}\right)^{3/2}, \tag{3}$$

where $\lambda_0$ is the laser wavelength. Under these conditions, the laser energy required to accelerate electrons up to the maximum energy can be written as

$$\varepsilon_{las} = 2\bar{\varepsilon}\left(\frac{P}{\bar{P}}\right)\gamma_{ph}, \tag{4}$$

where the characteristic energy $\bar{\varepsilon} = \frac{2\pi\bar{P}}{\omega}$.

Combining all of the above and assuming the optimized values of $a_0 \simeq 2.5$[41], the principal laser-plasma parameters can be rewritten as functions of $\varepsilon_{las}$ and scale as

**Electron energy:** $\varepsilon_m \approx 4.53 m_e c^2 (\varepsilon_{las}/\bar{\varepsilon})^{2/3}$

**Laser pulse waist:** $\omega_0 \approx 0.65\lambda_0(\varepsilon_{las}/\bar{\varepsilon})^{1/3}$

**Plasma density:** $n_e \approx 0.49 n_{cr}(\varepsilon_{las}/\bar{\varepsilon})^{-2/3}$

**Acceleration length:** $l_{acc} = 0.77\lambda_0(\varepsilon_{las}/\bar{\varepsilon})$

These values indicate that next-generation multi-kJ laser systems could access the multi-10-GeV to 100-GeV electron-energy range in a meter-scale accelerators. As an illustrative case, a 1 kJ, 1 $\mu$m wavelength laser could accelerate electrons up to approximately 140 GeV. The required electron density would be $\sim 1.6\times10^{16}$ cm$^{-3}$, the acceleration length would be 11.5 m, and the corresponding laser pulse waist and

Downloaded from https://www.cambridge.org/core. 19 Nov 2026 at 10:23:14, subject to the Cambridge Core terms of use.

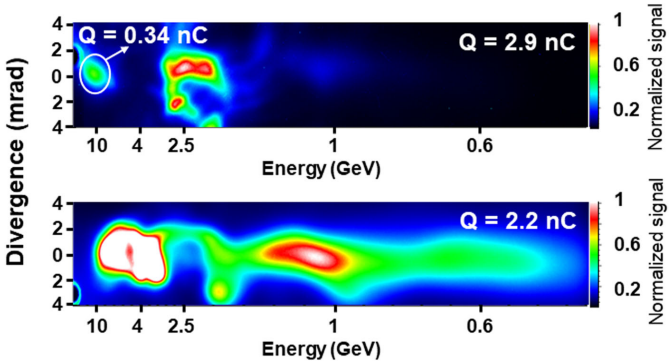



**Figure 2.** Figure taken from Aniculaesei *et al.*[20] showing the electron energy spectra of two energetic shots. The top spectrum shows a high-energy bunch with the centroid at 10.4 ± 1.9 GeV, a 3.4 GeV rms spread, a 340 pC charge (2.9 nC total charge), and a 0.9 mrad rms divergence. The bottom energy spectrum shows a 4.9 ± 0.4 GeV centroid electron bunch with a tail energy that extends beyond 10.4 GeV and has a 2.2 nC total charge with a 1.4 mrad rms divergence.

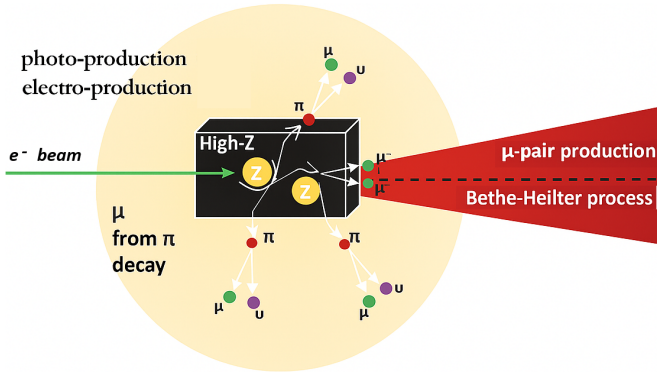



**Figure 3.** Simplified scheme[24] of muon production using an electron beam on a high-Z target. Muons produced by BH processes are boosted in the direction of the beam. Muons from $\pi$-decay are produced with a broader ($4\pi$) angular distributions

length are approximately 141 $\mu$m and 110 $\mu$m, respectively. These scaling laws provide the basis for estimating the performance of future laser-driven muon sources.

### 2.2. *Experimental demonstrations of multi-GeV LWFA electrons*

Owing to recent laser technology developments, several facilities have been able to demonstrate experimentally the production of multi-GeV electron beams, see Table 1. All these results have been realized by firing PW-class lasers into a $1-30$ cm long gas targets and driving plasma waves. It can be estimated, that a 1 PW laser can produce, $10^8$ electrons up to 10 GeV per shot. Electron beams with energy up to 10 GeV (see Figure 2) have also been demonstrated[20] with Nd:glass PW laser technology, which can deliver about five times more energy (130 J) in a longer laser pulse (130 fs) than with Ti:sapphire lasers. By focusing such a laser pulse on a 10 cm–long nanoparticle-doped gas target, high charge (340 pC), 10 ± 1.86 GeV electron bunches were generated. Higher charge bunches can be produced with lower energies as well. This approach was conducted with about 100 shots/day, but could be scaled to high-repetition-rate lasers ( ∼ 10 Hz).

LWFA electrons up to 10 GeV[18,19,21,45] were experimentally demonstrated using meter-scale, low-density, optical-field-ionized (OFI) plasma channels formed via self-waveguiding[46–52]. In this approach, a diffractive axicon is used to generate a Bessel beam that ionizes a plasma column in a gas sheet above a supersonic gas jet[53]. The subsequent hydrodynamic expansion forms an on-axis plasma "core" and an outward-expanding neutral-density shock. The leading edge of an intense LWFA drive pulse then ionizes this neutral shock, creating a refractive-index structure that guides the drive pulse as it propagates. The use of a plasma waveguide eliminates the laser intensity requirements for relativistic self-focusing, enabling acceleration to 10 GeV with <20 J of laser energy on target in a ∼60 fs pulse[19]. In general, this scheme can produce multi-GeV electron beams at repetition rates of a few hertz using an all-reflective optical setup allowing for >50,000 shots/day[54]. The recent demonstration[55] of 10 PW laser pulses with Ti:Sapphire technology at ELI Nuclear Physics (ELI-NP), and the planned 10 PW laser L4-ATON at ELI Beamlines (ELI-BL) (Nd:glass)[56], can enable electron beams in the multi-10s GeV energy range with nC charge at a 100 shots/day repetition rate[22].

## 3. Muons from multi-GeV laser-accelerated electrons: Production and Detection

As already mentioned, there are two principal ways to produce muons using high-energy electrons impinging on a high-Z target: (i) Pair production via BH process[15]: bremsstrahlung photons convert to $\mu^+\mu^-$ pairs, the resulting muons are more energetic and forward-peaked along the incident electron direction; (ii) $\pi$P: Photo- or electro-production of charged pions followed by their decay, the resulting muons have lower energies and broader ($4\pi$) angular distributions[13–15,24] (see Figure 3).

The generation of muons is accompanied by significant, high-flux secondary radiation background, including electrons, photons, and neutrons. These secondary particles, reach the detectors simultaneously with the muons and may cause saturation if not properly shielded. Consequently, an experimental challenge for LWFA-muons lies in reliably identifying muons against this intense background,but thanks to their high penetrating power, heavy shielding can be used. For example, a combination of Pb-impregnated concrete, lead, and plastic will help attenuate both the electron, photon, and neutron backgrounds with minimal effect on the muons. Figure 4 shows the yield of particles escaping a 2 cm thick tungsten target hit by a 5 GeV electron beam. The electrons, positrons and photons are

Downloaded from https://www.cambridge.org/core. 19 Nov 2026 at 10:23:14, subject to the Cambridge Core terms of use.

**Table 1.** Summary list of the petawatt-class facilities that reported the production of multi-GeV electron beams. Only facilities in operation are reported. Laser parameters are the ones reported in the associated references. An exhaustive list of petawatt-class facilities world-wide may be found in literature [57,58].

| Facility | Laser Technology | Laser Energy [J] | Laser Power [PW] | Accelerator Length [cm] | Electron Energy [GeV] | #Electrons per shot | |
|---|---|---|---|---|---|---|---|
| BELLA | Ti:Sapphire | 21 | 0.5 | 30 | 9.2 | $\sim 10^{7-8}$ | [18] |
| Texas PW | Nd:glass | 130 | 1.0 | 10 | 10 | $\sim 10^{9}$ | [20] |
| CSU (ALEPH) | Ti:Sapphire | 18 | 0.3 | 30 | 5–10 | $\sim 10^{8}$ | [19] |
| SULF | Ti:Sapphire | 20 | 1.0 | $\mathcal{O}(10)$ | 5 | $\sim 10^{8}$ | [59] |
| CoReLS | Ti:Sapphire | 83 | 4.2 | 5-10 | 5 | $\sim 10^{8}$ | [60] |
| CLF (Gemini) | Ti:Sapphire | 11 | 0.23 | 0.3-4.2 | 2.5 | $\sim 10^{9}$ | [61] |
| ELI-NP (1 PW HLPS) | Ti:Sapphire | 24 | 1.0 | 2 | 1-2 | $\sim 10^{8}$ | [62] |
| ELI-NP (10 PW HLPS) | Ti:Sapphire | 230 | 10 | 6 | 5-7 | $\sim 10^{8}$ | [63] |
| ELI-BL (L3-HAPLS) | Ti:Sapphire | 13 | 0.4 | 20 | 3–5 | $\sim 10^{7-8}$ | [54] |

the dominant contribution. These results were obtained using version 4-5.1 of the FLUKA Monte Carlo code [64–66] with the PRECISIO defaults and enabling muon pairs production. While code intercomparisons and physics-model dependencies are beyond the scope of this review, widely used transport codes such as FLUKA and Geant4 have undergone extensive experimental benchmarking and numerous intercomparison studies over several decades in accelerator, shielding, medical physics, and particle-transport applications. The reliability and validation of these codes for muon production and transport are discussed extensively in the literature [67].

Furthermore, the muon lifetime is a unique physical parameter $\tau_\mu = (2.1969811 \pm 0.0000022)\mu$s [5]. In laser-driven muon experiments, the observation of delayed decay signals following the prompt radiation burst, with a temporal distribution consistent with the known muon lifetime, provides strong evidence for the presence of stopped muons in the detector volume. Since the dominant prompt backgrounds generated in laser–matter interactions (electrons, photons, and neutrons) do not exhibit a characteristic decay signature on the ms timescale, lifetime measurements constitute a powerful and widely adopted diagnostic for muon identification. Nevertheless, lifetime measurements are most robust when combined with complementary observables such as particle directionality, penetration through shielding, energy deposition signatures, or agreement with detailed Monte Carlo simulations of the experimental configuration.

The most widely used muon detectors can be divided in three categories [4]: nuclear emulsion, scintillator, and gaseous detectors. Nuclear emulsions are very compact, easy to transport and install, and do not require electric power. For example, with a 1 cm stack, excellent spatial ($\mathcal{O}(10)$ $\mu$m) and angular ($\mathcal{O}(1)$ mrad) resolutions can be achieved. Drawbacks are: no online data as the emulsions need to be developed post exposure, expensive readout systems are required, and there is no timing information.

Scintillators and gaseous detectors provide real-time information with time resolution of $\mathcal{O}(1)$ ns. Modern gaseous detectors [68,69] reach time resolutions below 100 ps making them attractive for application in LWFA. These detectors are reusable and can work in a wide range of temperatures and pressures. Single detector units can be assembled together to cover large areas in the $\mathcal{O}(10)$ m$^2$, needed for large targets, *i.e.* volcanoes, bridges, nuclear power plants as explained in Sec. 4). To reach single-point spatial resolutions comparable to nuclear emulsions, these detectors need to be bulkier impacting their portability. Furthermore, they need power and robust readout electronics.

Existing muon detector technologies were primarily developed for cosmic-ray muography and high-energy physics applications. Cosmic-ray rates are low, while collider muon systems are typically located behind substantial calorimeters and absorbers. Consequently, detectors were optimized for low-event rates and low-background environments compared to laser-driven muon sources. Several groups are currently investigating the adaptation of established muon detection technologies to high-power laser facilities through dedicated shielding strategies, fast timing systems (ps-ns), and specialized triggering schemes. However, this effort is at an early stage and, at the time of writing, limited information is available in conference presentations and technical reports (https://doi.org/10.48550/arXiv.2605.13118). Dedicated detectors designed for laser-driven muon sources are only beginning to emerge. Commercial and academic initiatives are exploring compact detector concepts tailored to pulsed laser environments, but they not currently available and their performance remains to be studied and demonstrated experimentally.

The experiments reviewed in this paper are proof-of-principle demonstrations of laser-driven muon production. Their detector configurations were optimized to establish the presence of a muon signal under challenging background conditions rather than to maximize detection efficiency or provide complete characterization of the muon beam phase space. Future developments should focus on dedicated detector systems capable of operating in high-background

Downloaded from https://www.cambridge.org/core. 19 Nov 2026 at 10:23:14, subject to the Cambridge Core terms of use.

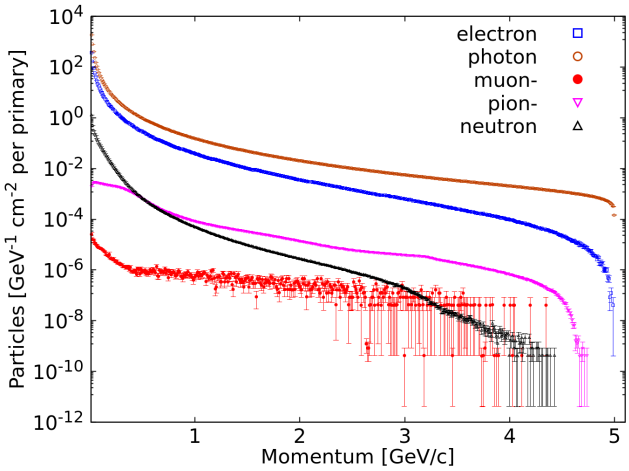



**Figure 4.** Yield of the particles escaping the target as a function of particle energy. The results were obtained simulating a 5 GeV electron pencil beam on a 2 cm thick tungsten target. The values are normalized per primary electrons. Spectra of positive particles are omitted for the sake of clarity. Simulations were performed using FLUKA version 4-5.1.

laser environments while providing measurements of muon yield, momentum, angular distributions, and particle trajectories with well-characterized efficiencies and uncertainties. Such developments will be essential for the transition from proof-of-principle demonstrations to application-oriented laser-driven muon sources. The following sections present these experiments in more detail, focusing on facility specifications, the electron source, muon converter geometry, and muon detection methodology. Plans for future studies at the ELI-NP and ELI-BL facilities are discussed as well.

### *3.1. The Texas-PW Muon experiment*

The first reported experiment aiming at demonstrating muon production with laser driven plasma electron accelerators was performed in Texas at the University of Texas at Austin on the Texas petawatt Laser (Texas-PW). The experiment was a collaboration between Texas, National Security Technologies (NST), Lockheed Martin, and National Energetics. The Texas-PW is a laser with unique specifications which make it particularly well suited for multi-GeV plasma electron acceleration with high charge per bunch (≈100 pC). The laser delivers up to 140 J in 130 fs pulses, higher energy than most petawatt-class Ti:sapphire lasers[70]. This optimizes production of muons because of higher charge per bunch when the plasma is driven in the "bubble" acceleration regime. In brief, it is a hybrid chirped pulse amplification system where the first stage of amplification (to 1 J) is performed in OPCPA crystals and the final energy is achieved in Nd:glass disk amplifiers. For these experiments the compressed pulse, with nearly flat-top spatial profile, was directed into a long chamber, with a 10 m (f/40) focusing optic which weakly focused the pulses into a 7 cm long He gas cell where electron acceleration took place. This yielded a plasma density (of doubly ionized He) of about $5 \times 10^{17}\ cm^{-3}$. The production of multi-GeV electrons on the TPW has been well characterized by the Texas experimental team of M. C. Downer[71–74]. In these muon production experiments the electron energy averaged 2 GeV but varied shot to shot from 1 to 3 GeV. The charge per bunch was roughly 100 pC. Half a meter downstream, a 1.1 T magnet was placed to disperse slightly the GeV electron beam which was imaged with a Charge-Coupled Device (CCD) sensor and image plate. The team placed a 2.54 cm thick tungsten muon converter 2 m down from the acceleration cell. The target thickness was chosen based on simulations at the University of Texas by T. Ditmire.

The team also ran Geant4[75] simulations assuming 2 GeV electrons and 65 pC of charge (on the low side of the actual experimental production). Geant4 predicted a couple of thousand muons per shot emitted in a cone with half maximum half cone width of about 30°. The Texas-PW team employed two different types of muon detectors deployed in the expected cone of muons[76]. The first detector was a drift tube tracker manufactured by Decision Sciences International. This detector consisted of 96 aluminum tubes arranged in layers of 24 filled with gas composed of a mixture of He and Ar and a center anode wire. It was situated at the far end of the Texas-PW high bay, roughly 30 m from the tungsten converter behind the 3 foot thick Pb impregnated concrete shield wall and a 2 inch lead shield. This first detector suffered saturation and meaningful data was obtained only from a handful of laser shots. The second detector was a 1 cm thick 60 x 60 $cm^2$ sheet of Eljen EJ-260 scintillator placed behind a stepped wedge of lead with varying thickness up to 12 inches. The team observed on roughly 40 laser shots, an inferred average of 1000 muons per shot. The detectors were arranged at various places in the forward cone of the electron beam. From this, a rudimentary measurement of the muon angular distribution was derived. Figure 5 illustrates data from these shots. These show inferred muon yield at three angles averaged over 10 shots, 0°, 13° and 24° from the electron beam forward axis. These data indicate that the forward directed muon emission is in a cone of about 25° half width at half maximum consistent with the Geant4 results.

### *3.2. Demonstration of muon production at SULF*

To address the growing demand for high-energy electron beams in advanced radiation research, the Shanghai Institute of Optics and Fine Mechanics (SIOM) established a high-energy laser wakefield acceleration (LWFA) platform, which became fully operational in 2020. The system is based on the 1 PW, 0.1 Hz laser of the Shanghai Superintense Ultrafast Laser Facility (SULF)[77,78]. Laser pulses with energies of 15–24 J are tightly focused into gas targets inside the electron acceleration chamber using an f/60 optical

Downloaded from https://www.cambridge.org/core. 19 Nov 2026 at 10:23:14, subject to the Cambridge Core terms of use.

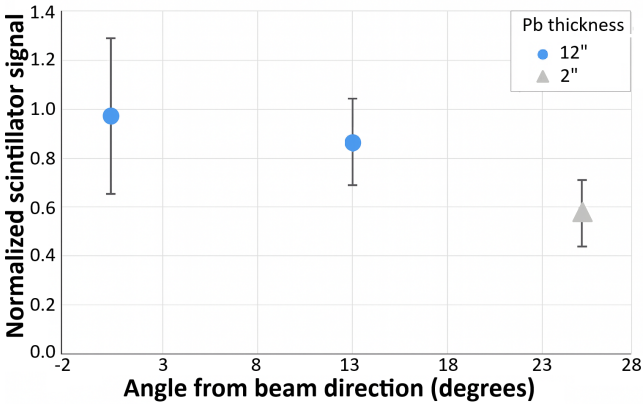



**Figure 5.** Data illustrating inferred angular distribution of muons in the direction along the laser plasma accelerated electron beam. The plot shows the normalized scintillator signal vs angle of screen position with respect to electron beam input to the tungsten beam dump

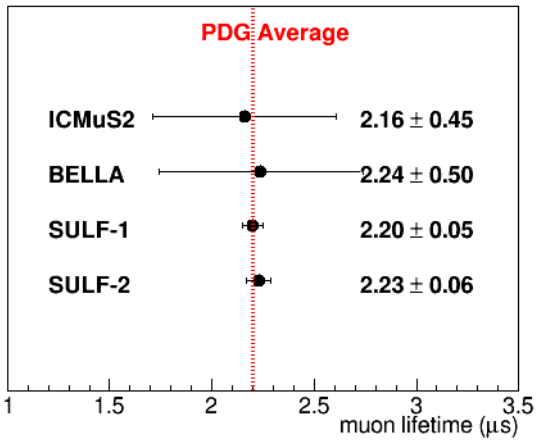



**Figure 6.** Summary of the measured values of the muon lifetime at BELLA, ICMUS2, and SULF. The vertical red band shows the Particle Data Group (PDG) average value of $2.1969811 \pm 0.0000022$ $\mu$s [5].

system with a 12 m focal length. The focal spot had a full width at half maximum (FWHM) of approximately 59×59 $\mu$m$^2$, corresponding to a normalized laser amplitude $a_0$ between 1.2 and 2.2. Two types of gas targets were used to accommodate different experimental requirements: capillaries (3–6 cm in length) and elliptical nozzles (8.8 mm in length), producing plasma densities in the range of $10^{17}$–$10^{19}$ cm$^{-3}$. The resulting high-energy electron beams were analyzed with a magnetic spectrometer with an effective field length of 1.8 m and a maximum magnetic field strength of 1.5 T. Electron energy spectra were recorded using fluorescence screens coupled to CCD imaging, and the tunable magnetic field allows precise characterization of beams over a broad energy range, from 0.2 to 20 GeV.

A comprehensive series of experiments at SULF explored a range of plasma density profiles, consistently producing GeV-class electron beams across varying acceleration conditions. Using capillary targets, electron beams with energies exceeding 5 GeV and average charges of ∼20 pC were achieved, while gas nozzles yielded highly reproducible beams in the 0.4–1.5 GeV range with average charges of ∼200 pC. This stable and tunable electron beam was ideal for laser-driven muon production.

An experiment[24], was conducted to identify the muon signal at SULF by measuring the particle lifetime. The laser energy reaching the He gas target was approximately 15–20 J, with a pulse width of about 30 fs, a wavelength of 800 nm, and a repetition rate of 0.1 Hz. A total of 178 shots were collected with an average electron charge of 200 pC/shot. When these high-energy electron beams interacted with a lead conversion target, muons and pions were produced. These secondary particles subsequently came to rest within the surrounding lead shielding or on the inner surface of one of two liquid scintillator detectors positioned behind the lead. The electrons and positrons resulting from their decay were detected by scintillators, enabling the measurement of the muon lifetime. The experimental results showed that the measured muon lifetime is in excellent agreement with the established literature value, thereby providing experimental evidence of muon production (see Figure 6). Further analysis of the angular distribution of the emitted muons indicated that they originate predominantly from pion decay, with an estimated production efficiency of approximately 0.01 $\mu$/e.

### *3.3. Generation and characterization of directional muon beams at BELLA*

At the Lab Laser Accelerator (BELLA) Petawatt center, a 40 fs laser pulse with 21 J of energy and a 53 $\mu$m focal waist was coupled into a 30 cm-long OFI hydrodynamic channel and guided via self-waveguiding[50]. This configuration produced broadband electron bunches with charges of approximately 80 pC for energies above 2 GeV, extending up to 8 GeV, and featuring sub-mrad divergence with a 3 mrad shot-to-shot pointing jitter[18]. The electron beams were directed onto a composite high-Z beam dump, consisting of layers of lead and steel followed by concrete, which absorbed most of the secondary radiation. In this configuration, BH pair production of $\mu^+\mu^-$ pairs occurred within the shielding materials[6,16]. The resulting muons exhibited energies up to that of the primary electrons and were emitted within narrow angular cones, characteristic of their directional production mechanism. Due to their strong penetration power, a fraction of these muons traversed the shielding while retaining several GeV of energy. They were detected using a pair of synchronized scintillator-based radiation detectors positioned along and off the beam axis. Each laser shot generated time-delayed scintillation signals corresponding to muon decays, with an average lifetime of $\tau = 2.2 \pm 0.5 \mu$s (see Figure 6). Accumulating delayed events over 760 laser shots yielded a total of $126 \pm 12$ identified

Downloaded from https://www.cambridge.org/core. 19 Nov 2026 at 10:23:14, subject to the Cambridge Core terms of use.

muons[25]. Geant4 simulations of the full experimental geometry, including the beam dump and shielding, reproduced the measurements and clarified the origin and angular distribution of the detected muons[75,79,80]. Simulations confirmed that muons emitted along the beam axis predominantly originate from the BH process, resulting in a highly collimated and energetic forward-directed beam. In contrast, measurements and modeling of off-axis detectors revealed an additional, quasi-isotropic muon component generated via pion decay[15].

### 3.4. *The Intense and Compact Muon Sources for Science and Security Experiments at ALEPH*

The Intense and Compact Muon Sources for Science and Security (ICMuS2) collaboration, led by LLNL, has advanced the development of compact, laser-driven muon sources for applications. This work includes the development of next-generation laser driver technology[81], scaling laser-driven muon generation schemes to 100 GeV energy at application-relevant fluxes[22], the development of imaging applications using artificially generated muon beams, and the experimental investigation of muon production (paper in preparation). Laser-driven muon production was demonstrated (see Figure 6) using the ALEPH facility[82] at CSU by the multi-institutional team consisting of members from CSU, LLNL, ELI-BL, and the University of Maryland (UMD). In addition, a proof-of-principle imaging demonstration employing high-energy particle beams, including muons, generated by laser-accelerated, multi-GeV electrons was performed[? ].
At ALEPH, LWFA drive pulses of 200–300 TW and $\sim$ 60 fs duration have been focused into optical field ionized plasma waveguides formed in a supersonic hydrogen gas jet[53] with self-waveguiding, enabling acceleration over distances of 20–30 cm. Nitrogen doping of the gas jet was employed to facilitate ionization injection of electrons. Uniform doping resulted in multi-peaked spectra due to stage-II mode beating, while localized doping produced quasi-monoenergetic beams with an energy spread below $10\%$[83]. Since 2022, beam energy and charge have been progressively enhanced through optimization of laser and waveguide parameters ƒ including pulse duration, plasma density, matched mode size, and channel length[49]. Recent experiments have demonstrated stable production of multi-GeV beams with nanocoulomb-level charge, as well as picocoulomb-level signals in the 10 GeV energy range[19,84–86]. The system is capable of delivering up to 1000 multi-GeV beams per day at a repetition rate of 0.1 Hz. Electrons accelerated to up to 10 GeV[19] were directed onto a $\sim$ 100 mm-thick tungsten entrance slit of a magnetic spectrometer. This spectrometer was used to characterize the charge, energy, and beam profiles of the electron beam. The tungsten entrance slit also served as the high-Z converter target, producing muon pairs via photo-produced pion decays and BH photo-produced pairs, as well as other secondary particles, enabling simultaneous characterization of electron beam energy spectra and measurement of secondaries. To detect the decays of laser-generated muons, a dedicated detector was placed downstream of the magnetic spectrometer along the beam axis. This detector consisted of a 127 mm-diameter photomultiplier tube (PMT) coupled to a 75 mm $\times$ 150 mm $\times$ 300 mm block of EJ-200 scintillating plastic. It was shielded with lead and polyethylene, with 350 mm of lead positioned between the detector and the tungsten converter to attenuate the primary electron beam and other radiation. The relative delays of signals detected more than 1 $\mu$s after the main pulse were recorded during a single experimental day. These delays exhibit approximately an exponential decay, with a best-fit time constant of 2.16 $\mu$s, consistent with the muon lifetime value reported by the PDG[5].
A separate proof-of-principle imaging demonstration was also conducted to show the potential for through-wall imaging using laser-generated muons and other high-energy particles. A coarse, pixelated detector array was placed inside a truck located outside the laboratory, aligned with the beam axis. This remote array consisted of scintillators coupled to silicon photomultiplier detectors (SiPMs). It detected signals from a single shot of the laser-driven beam, even through the laboratory's interior and exterior walls and associated radiation shielding. A coarse imaging test was performed by blocking two detectors with lead bricks of 24 inches, which nearly extinguished the detected muon signals. While the detector used by the team had limited particle discrimination, these results demonstrated the feasibility of remote imaging using laser-driven muons and related high-energy particles[? ].

### 3.5. *LWFA muon at ELI-NP with a PW-class Laser*

At ELI-NP in Romania, the recently commissioned 1 PW laser (24 J, 24 fs), which is part of the High-Power Laser System (HPLS), was also used to demonstrate production of multi-GeV electron beams, accelerated in cm-scale plasma channels with nC-scale electron beams using oversize laser focal spots.[62]. Extensive numerical modeling and optimization of the muon source driven by these electron beams was reported, together with a proof-of-principle design of a transport and manipulation line[87]. These numerical models indicate that a suitable beamline driven by a PW-scale laser would be capable of delivering more than 100 muons per nC of primary electron beam at the detector plane, in a few $cm^2$ area. Muon sources of this kind could be implemented in high-power laser facilities currently under construction, such as Extreme Photonics Applications Centre (EPAC) at the Center Laser Facility (CLF)[88] and the European plasma accelerator facility EuPRAXIA[89]. These numerical results were validated in an experimental campaign at ELI-NP[87]. The PW-class laser was focused using an f/26 off-axis parabola at the edge of a 20mm gas-jet filled with a helium gas doped with $2\%$ nitrogen. The interaction produced

Downloaded from https://www.cambridge.org/core. 19 Nov 2026 at 10:23:14, subject to the Cambridge Core terms of use.

electron beams with a broad energy spectrum extending up to 2 GeV and an overall charge above 200 MeV of (560 $\pm$ 180) pC. The electron beam impinged on Pb targets of variable thickness between 1-2 cm. Statistically significant evidence of muon production was observed using TimePix3 detectors[90,91] in a suitable shielding configuration, in excellent agreement with numerical predictions. This proof-of-principle demonstrator provides a basis for future design and installation of laser-driven muon beamlines at high-power laser facilities. Extension of these results to 10 PW laser systems suggest the possibility of muon fluxes exceeding the current results by more than an order of magnitude, but at a cost of a slower repetition rate (as explained in the following section 3.6).

### *3.6. LWFA muon at ELI-NP with a 10 PW-class Laser*

HLPS at ELI-NP, introduced in the previous section, is also capable of delivering a 10 PW laser pulse[55] with central wavelength of 810 nm and pulse duration as short as 23 fs. The laser can be focused to a spot of $\sim$60 $\mu$m at FWHM by an f/60 spherical mirror[92]. This laser was used to investigate the generation of muons as secondary radiation[93]. The primary electron beam was generated via the LWFA mechanism by shooting onto a 60 mm long gas jet target, without guiding[63]. The generated electrons had a peak energy of $\sim$ 4 GeV and a beam charge exceeding 1 nC. The high-energy electrons were sent to a secondary target, a 40 cm thick target made of lead bricks, which acted as a converter for the generation of the high-energy, collimated muons via the BH process, and low-energy and highly diverging muons via pion generation and subsequent decay[87]. During the interaction, a large amount of secondary particles like gammas, pions, electrons, and neutrons were generated in addition to the muons. This presented a difficulty in detecting and characterizing the high-energy muons because of the high background level. A large muon detector was installed far outside a shielded experimental area[75]. This configuration reduced the secondary particle flux on the detector, both because of the large distance between the detector and the converter ($\sim$10 m) and also owing to the 2 m thick concrete wall between the experimental area and the detector. The muon detector was a $1\times1$ m$^2$ muon telescope originally designed for muography applications using cosmic-ray muons and capable of reconstructing individual particle trajectories. The detector consisted of 4 layers of 36 scintillator bars, each read by a wavelength-shifting fiber and a SiPM[94,95]. Accurate reconstruction of muon trajectories requires a low rate of events, but the device can also record the shape of an incoming particle bunch. Placing the detector far from the muon source took advantage of the natural spread of the muons, which was $\sim$2 m at the location of the detector. Although a high background was still present, and more shielding was needed, preliminary results indicate that the detector recorded multiple events corresponding to muons of energy up to or exceeding 1 GeV. Data analysis is ongoing. Future plans at ELI-NP include continuing the measurements of multi-GeV muons and their characteristics using the same as well as different detectors, while improving shielding and optimizing experimental setup.

### *3.7. ELI-BL: Muon Production Capabilities and Future Plans*

The ELI-BL user facility houses four main laser systems that serve a dozen experimental stations providing users with photons, electrons, and proton beams[96]. Since 2024, it has also accepted user proposals for muon generation and detection using the L3-HAPLS[97] (High-Repetition-Rate Advanced Petawatt Laser System) PW-class laser. L3-HAPLS is designed to deliver laser pulses with 30 J energy and 30 fs duration at a repetition rate of 10 Hz and a central wavelength of 810 nm. L3-HAPLS serves, among other stations, the Electron Beam Accelerator[98] (ELBA) experimental station for fundamental science. ELBA is equipped with a 10 m focal length off-axis parabola to focus the L3-HAPLS laser pulses down to 40 $\mu$m onto in-house developed supersonic gas jets[99,100]. This allows L3 to drive LWFA in a linear regime. By using a pick-off mirror on the compressed laser beam, $\sim$1 J of laser energy is used to create an all-optical plasma channel used to extend the acceleration length. Electron beams up to 5 GeV with 13 J, 30 fs laser pulses at 0.2 Hz repetition rate have been produced[54]. High power laser guiding has been achieved at 3.3 Hz with up to 8 J laser energy, paving the way for near future multi-GeV beams at 3.3 Hz. A 2 m concrete beam dump acts as an electron-muon converter. After the beam dump one can access a 20 m long, 7 m wide area to place detectors, triggering systems and possible extra shielding. The estimated muon flux at this facility is shown in Figure 7. A future upgrade of ELBA based on the 10 PW laser L4-Aton[101] has been designed. It consists of a 65 meter long off-axis parabola focusing down the 1.5 kJ, 150 fs laser pulses to 120 $\mu$m focal spot. This set-up will enable electron beam energies well above 10 GeV, potentially reaching up to 100 GeV[22].

**Comparison of current experimental demonstrations.** All the experiments reviewed above, schematically summarized in Table 2, should be regarded as proof-of-principle demonstrations of laser-driven muon production and not as mature muon beamlines. Their principal objective was to establish the generation and detection of muons from laser-plasma-accelerated electron beams rather than to optimize source performance. Consequently, key source parameters such as absolute muon yield, energy spectrum, angular divergence, emittance, and overall conversion efficiency were not systematically measured under comparable conditions. Direct quantitative ranking of the different approaches

Downloaded from https://www.cambridge.org/core. 19 Nov 2026 at 10:23:14, subject to the Cambridge Core terms of use.

**Table 2.** Summary of relevant parameters laser-driven muon production experiments that have been presented in this review. Full details may be found at [23–26] and https://arxiv.org/abs/2607.12984.

| Experiment | Electron Energy [GeV] | Electron Charge [pC] | Target Material | Estimated Muon Yield [#/shot] | Muon Identification Technique | Muon Detector Type |
|---|---|---|---|---|---|---|
| Texas PW | ∼2 | 100 | W | N.A. | N.A. | Drift tubes and Scintillator |
| SULF | 0.4-1.5 | ∼200 | Pb | $< 10^7$ | Lifetime | Liquid scintillator |
| BELLA | 2-8 | ∼80 | Pb,Steel,Concrete | $2.6 \cdot 10^4$ | Lifetime | Scintillator |
| ICMuS2 | <8 | >100 pC | W | $4 \cdot 10^4$ | Lifetime | Scintillator |
| ELI-NP (1 PW) | <2 | ∼560 | Pb | N.A. | Track Identification | Solid state |

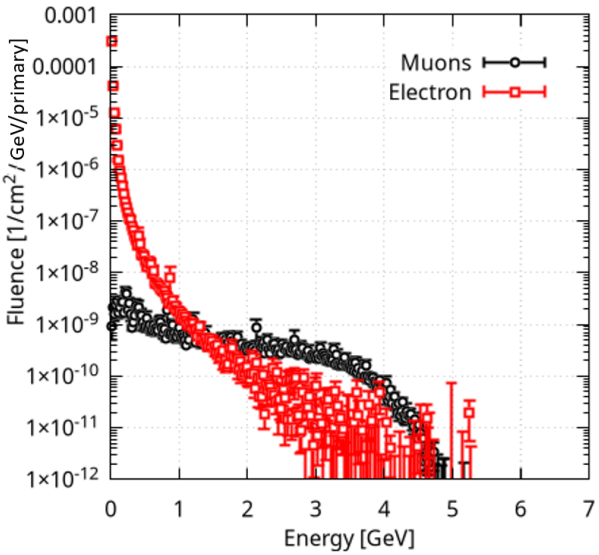



**Figure 7.** Estimated muon flux 0.5 m after the ELBA dump. The results are normalized per primary electron particle, with 5 GeV energy. Results were obtained using FLUKA Monte Carlo code.

is therefore premature. Instead, the existing experiments demonstrate complementary operational regimes, ranging from high-charge electron beams favoring larger per-shot particle production to higher-repetition-rate systems offering enhanced average flux. A systematic assessment of how source performance depends on laser architecture, electron beam properties, converter design, detector configuration, and repetition rate remains an important objective for future studies. Such an assessment should combine dedicated experimental campaigns with validated Monte Carlo simulations to establish reliable performance metrics and optimization strategies. Ultimately, the most suitable source configuration will depend on the intended application, since different use cases place different requirements on muon energy, flux, directionality, timing structure, and source compactness, as discussed in section 4.

## 4. Applications of LWFA-Driven Muons

Applications of muons and muon beams are numerous. This is because of the relatively long muon lifetime, high penetration power and known correlation between the amount of multiple Coulomb scattering that occurs along its trajectory and the material properties. The amount of scattering is proportional to the thickness, density, and atomic number (Z), and is inversely proportional to the muon momentum. The statistical nature of multiple scattering allows for the parameterization of the projected scattering angle distribution as a Gaussian with a width of

$$\sigma \cong \frac{13.6MeV}{\beta cp}\sqrt{\frac{L}{\chi_0}}\left[1+0.038ln\left(\frac{L}{\chi_0}\right)\right] \qquad (5)$$

where $\beta c$ is the muon speed, $p$ is the muon momentum, $L$ is the path length through the scattering material, and $\chi_0$ is the radiation length of the scattering material [102]. The scattering angle can be measured by tracking the muon before and after passing through a volume of interest using position sensitive detectors (see Figure 8). This technique, based on the scattering angle of the surviving muons, is referred to as scattering muography (also referred to as muon tomography). It has the attractive advantage of providing 3-D tomographic images of the inspected materials, but is suitable to investigate volumes with dimensions not exceeding tens of meters.

For larger objects, transmission muography is preferred. This technique is based on the measurement of the attenuation of the muons flux. If the initial muon flux is known, the measurement needs to be done only after the object. Therefore, only one set of detectors is needed. A good overview of the state-of-the-art in muon applications can be found in Bonomi *et al.* [103].

One benefit associated with the use of artificial muon sources, is the potential control over the flux of muons. LWFA facilities can produce semi-collimated beams of muons in a horizontal direction. Furthermore, based on recent experimental demonstrations [25], this flux may be ∼10,000× higher than the natural cosmic ray flux at large zenith angles. Since scattering tomography systems track

Downloaded from https://www.cambridge.org/core. 19 Nov 2026 at 10:23:14, subject to the Cambridge Core terms of use.

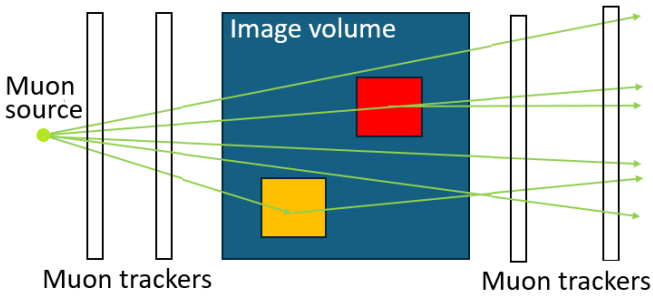



**Figure 8.** Conceptual drawing of an artificial muon-based scanning system.

individual muons, ensuring an efficient balance between the muon rate through such a system and pile-up is crucial. For large conventional muon scattering tomography detectors, the incident flux of muons spans a wide angular range, and, therefore, tracking ambiguities are not difficult to resolve for uncorrelated coincident events. In contrast, multiple muons with nearly identical incident directions, but not necessarily identical initial momenta, could be challenging to deal with although still useful for radiography applications.
The following sections present examples of potential applications of LWFA muons.

### *4.1. Nuclear Safety and Homeland Security*

Muon tomography can be an invaluable and non-destructive tool for safety and security agencies at seaports, airports, border control, critical infrastructure, sensitive locations, and nuclear and radioactive sites. The high penetration power and multiple Coulomb scattering of the muons can be used for the detection of well-shielded nuclear contraband as well as the detection of problems within nuclear power plants and spent nuclear fuel storage[104]. Unfortunately, the momentum spectrum of cosmic ray muons is broad, which, without direct measurement, can lead to large systematic uncertainties on the reconstructed scattering density of a target. It has been shown that direct measurement of the muon momentum improves the probability of detecting targets and improves the quality of reconstructed images[105,106]. An artificial muon source with a tunable momentum spectrum would provide flexibility in nuclear safety and border and national security applications of muon scattering and attenuation tomography. Finally, beyond the benefits of an artificial muon source by itself, a LWFA facility also produces ample additional secondary particles (photons, electrons and positrons, and neutrons), and can also provide an external trigger signal for timing purposes. Such a trigger could be used to detect the production of muon-induced neutrons through muon capture on high-Z nuclei which further enhances the discrimination of Special Nuclear Materials (SNM)[107]. This would facilitate imaging of SNM-containing objects tagged using muon tracking detectors located outside the objects, and may have potential applications in warhead verification. In addition, the flux of neutrons from the LWFA beam dump could be used in lieu of existing deuterium-deuterium (D-D), deuterium-tritium (D-T), and $^{252}$Cf neutron sources for active interrogation applications which are employed for detecting special nuclear material and certain types of contraband.
Conceptually, an artificial muon-based scanning system for nuclear and homeland security would require either one set of trackers (attenuation tomography) or two (scattering tomography) oriented vertically to detect the near-horizontal muons produced by the LWFA. Existing cosmic ray-based systems could be easily supplemented with additional detectors to utilize both natural and artificial muon sources from laser-driven accelerators, simultaneously providing additional flexibility. Another security application of a compact pulse muon source would be to image tunnels and cavities underground. This follows on the pioneering work of Alvarez et al.[108] who used cosmic ray muons to look for hidden chambers in the pyramids. Modern day applications would include fast detection of tunnels being burrowed under sensitive areas (military installations or border areas)[109,110]. A mobile laser-driven muon source coupled with buried muon detectors could detect new tunnels within minutes of interrogation of that region of land.

### *4.2. Muons for Geology and Archaeology*

The noninvasive nature of muons and their ability to penetrate deep into matter make muon-based imaging a promising tool for various geoscience and archaeology projects. In earth sciences, muography has already proven its worth in the study of both dormant and more dynamic, active volcanic systems[111], yielding insight in many features including conduit sizes, plug formation and explosion, hydrothermal change in lava domes and more. Meanwhile applications also appear in cave mapping[112], groundwater flow studies[113], mining operations, carbon capture and storage monitoring[114], and several more areas. In archaeology, it has opened new avenues for discovering and documenting hidden structures within ancient monuments, with e.g. the aforementioned Alvarez's experiment[108] at the Khafre pyramid and the famous ScanPyramids missions[115] at the Great Pyramid of Khufu in Egypt using multiple muon detectors located inside and outside the structure. Other examples of archaeological sites that have been explored using similar techniques include the Pyramid of the Sun in Mexico[116], the Xi'an Defensive Walls in China[117], the Palazzone Necropolis Etruscan tombs[118] and early settlements of the city of Naples at Mt. Echia in Italy[109], the ancient Apollonia tumulus in Greece[119], and several more. Muographic techniques have also been proposed to monitor structural stability of heritage buildings, such as the Palazzo della Loggia in Italy[120], where muons can be used to track deformation in a wooden vaulted roof.
A more recent idea is to extend the use of muon imag-

Downloaded from https://www.cambridge.org/core. 19 Nov 2026 at 10:23:14, subject to the Cambridge Core terms of use.

ing to smaller (meter-scale) cultural artifacts[121], where both absorption and scattering-based muography could help, studying internal features or water content in statues, in cases where traditional techniques like X-ray or neutron imaging are limited due to size, fragility, or safety concerns, or where moving fragile or immobile items is a limiting factor.

A common feature in these projects is the use of transmission muography, where the typical dimensions involved vary depending on the specific target, from a few meters up to kilometer-scale in terms of object size and thus material that muons need to traverse (e.g. buildings, volcanoes), distance between target and muon detectors, and in case of underground applications, amount of rock or soil muons have to penetrate before reaching the target. This often severely limits the detectable cosmic muon flux and imposes a minimum energy (going from GeV to sometimes TeV scale) for muons to reach the telescopes. Given the azimuthal dependence of the cosmic muon flux, typical muography setups place the muon detectors looking upward from below the target to exploit the flux to the maximum possible and limit the acquisition time.

Given the complexity of traditional cosmic muon imaging campaigns, with the large variety of targets and setup geometries, deriving general quantitative criteria for the use of laser-driven sources in geoscience and archaeology imaging applications is not trivial. Case-by-case considerations about the setup geometry, detector and source placement, desired accuracy, data acquisition times and environmental conditions, and more will be required. Nonetheless, the high muon flux values these sources bring and the option to tune both the flux and muon energy range could address some of the limitations one faces with the cosmic muon flux that currently impede imaging speed and achievable resolution for various applications. The latter is particularly true for projects with horizontal setups or highly dynamic targets. Considering also geometries with underground targets, the directionality of a laser-driven muon source and its tunability of the angular aperture can be very helpful to reach and fully illuminate targets. Laser-driven muon sources could provide a advantages in projects involving, for example, easily reachable targets above ground (i.e. buildings, monuments) or small-sized cultural heritage objects that can be moved into the lab. Furthermore, setups where traditional cosmic muon data from multiple telescopes placed at different locations around the target are combined to derive 3D information of the object (see e.g. Miyamoto *et al.*[122]) could also benefit from mobile, high-flux muon sources with short acquisition times. Before moving to practical applications, issues as accurate determination of the muon source flux, beam-induced backgrounds, rate capability of the muon detection systems, power consumption at remote locations, and more will have to be addressed.

### *4.3. High Energy Physics: Precision Measurements, Detector Studies and Discoveries*

Muon beams are valuable tools for both the present and the future of experimental high-energy physics (HEP). Their applications span precision studies of fundamental physics, the development of next-generation collider concepts, and their use as test beams for detector characterization and optimization—each of which requires very different beam characteristics and accelerator configurations. In the domain of fundamental physics, muon beams can enable precision measurements of Standard Model parameters and sensitive searches for forbidden or highly suppressed processes. These include the anomalous magnetic moment of the muon[123], ultra-rare decay channels[124], and the study of exotic bound states such as muonium and muonic atoms[125]. Such experiments typically demand extremely high muon fluxes at low momenta to maximize sensitivity. At the same time, interest in muon colliders has risen strongly within the HEP community. Studies submitted to the 2020 update of the European Strategy for Particle Physics (ESPP) highlighted the potential of such machines[126], while more recently, an electron–muon collider has been proposed at the high-energy accelerator research organization KEK as a complementary approach[127]. However, realizing these concepts requires major advances in muon beam brightness, cooling, and rapid acceleration, as well as solutions to significant technological challenges, some of which can be addressed at smaller-scale facilities.

Beyond colliders, intense muon beams are also central to neutrino factories, where muon decays produce controlled, high-intensity neutrino beams for oscillation experiments. Emerging techniques, such as ionization cooling and advanced target concepts, promise to enhance both the quality and yield of such beams. Finally, muons play a critical role as test beams for detector research and development. Thanks to their behavior as minimum-ionizing particles at energies above a few hundred MeV, muons serve as excellent "standard candles" for calorimeter calibration and highly reliable probes for tracking detectors. For these applications, beams in the GeV energy range are typically required, with relatively low rates (kHz/cm$^2$) and limited angular divergence. Finally, Higgs factories require a center-of-mass energy of $\sim$ 126 GeV[128,129]. Colliding LWFA-muon beams of 65-70 GeV would comfortably exceed this threshold. In this broader context, laser-driven muon sources could open new opportunities across these domains. These compact, high-flux muon sources could complement conventional accelerator facilities. For precision physics, in fact, laser-based muon beams could provide dedicated, tunable sources at relatively low cost, enabling systematic studies of muonic atoms or rare decays in smaller-scale laboratories. In collider research, laser-driven schemes might serve as injectors or testbeds for advanced muon cooling and beam manipulation concepts, reducing reliance on large-scale in-

Downloaded from https://www.cambridge.org/core. 19 Nov 2026 at 10:23:14, subject to the Cambridge Core terms of use.

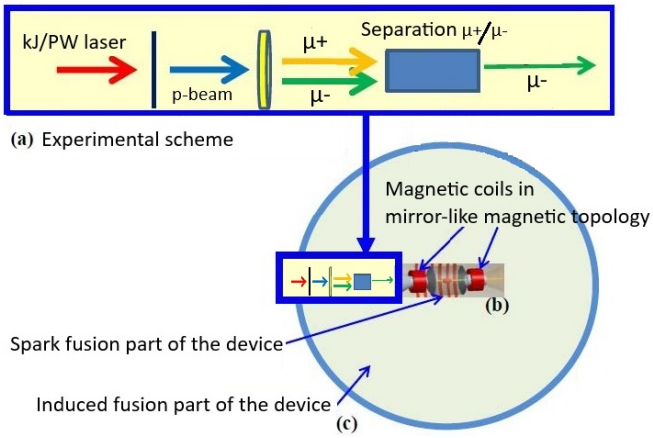



**Figure 9.** Potential experimental configuration for muon catalyzed fusion at a high-power laser facility. The proposed example assumes muon ($\mu$) production by proton (p) beam on a solid target.

frastructure in early R&D. For neutrino science, laser-based muon production could help prototype compact neutrino sources, supporting detector calibration and cross-section measurements. Finally, in detector development, laser-driven, muons—delivered short, intense bursts synchronized with a high-power laser system could provide unique test conditions for fast-timing calorimetry and radiation-hard tracking technologies. Taken together, these applications underline the unique role of laser-driven muon beams across the HEP landscape.

### *4.4. Muon Catalyzed Fusion*

Muon-catalyzed fusion ($\mu$CF) is a process by which nuclear fusion can be aided at ion temperatures significantly lower (even room temperature) than those required for thermonuclear fusion[130–132]. $\mu$CF is of interest, because of its potential application to fusion ignition, for very low initial temperatures ($T_{in}$) $<$ 100 eV of deuterium-tritium (D-T) or deuterium-deuterium (D-D) fuel. In the same context, the possibility of fusion ignition from at $T_{in}$ $<$ 100 keV of the proton-$^{11}$B (p-$^{11}$B) medium, presents a significant breakthrough in the field of aneutronic fusion.

In the case of $\mu$CF of D-T and D-D, muons are forced into hydrogen isotopes close enough for it to be captured. Since the muon is 207 times heavier than the electron, the resulting nuclei are drawn 186[133] times closer than in a normal hydrogen isotope. When the nuclei move closer together, the fusion probability increases, to the point where a significant number of fusion events can happen at room temperature. Unfortunately, current muon production methods require more energy than what can be produced by the resulting fusion reactions, making this process inefficient. In this context, LWFA may provide a comparatively cheap and intense muon source for energy production $\mu$CF. Additionally the desired number of muons for fusion applications is $\sim 10^{11-12}$ per shot, predicted in some LWFA scenarios especially at the low energies needed for $\mu$CF. The difficulties of achieving effective $\mu$CF in D-T or D-D medium are related not only to the challenges of producing a high number of muons, but also to increasing the number of the induced fusion reactions per muon. This is due to (i) the finite life-time of the muons and (ii) the sticking effect of muons with the produced helium from the (D+T) nuclear reactions, which reduces the number of $\mu$CF reactions to ∼300 fusions/muon. To overcome these difficulties, a new configuration is proposed[134] with two distinct parts, operating in succession (see Figure 9). In the first step, the generated muons ($\sim 10^{11}$) interact with the initial low temperature ($<$ 100 eV) D–T plasma ($\sim 10^{20}$ cm$^{-3}$), that is trapped in the "fusion spark part" (∼1 cm$^3$) of the configuration for a duration of 1-2 $\mu$s. In the second step, the induced $\mu$CF produces a sufficient number of alpha particles to ignite fusion. This happens by alpha heating effect in the main fusion part of the configuration, that contains the low-density ($\sim 10^{16}$ cm$^{-3}$) D-T medium with $T_{in} \sim 800$ eV.

Proton-$^{11}$B fuel is attractive, not only because of its aneutronic nuclear fusion reaction, but also because it does not need breeding technologies for the production of its fuel components; hydrogen and boron are abundant in nature. The main hurdle for fusion ignition of the p-$^{11}$B medium is that its nuclear reaction cross section is only efficient for higher energies than 250 keV. Numerical simulations[135] show that the addition of energetic protons (700 keV or higher) in a p-$^{11}$B medium with low $T_{in} \sim 20$ keV and density $\sim 10^{20}$ m$^{-3}$, sparks fusion ignition, with an output power density of a few MW/m$^3$. The required high density ($10^{19-20}$ m$^{-3}$) of the energetic protons could be generated, using a mixture of deuterium and p-$^{11}$B fuel. Unfortunately, "direct" $\mu$CF of p-$^{11}$B is orders of magnitude less efficient[130,131] than the corresponding $\mu$CF of D-D or D-T. In this case, the employment of the $\mu$CF configuration, described in the first section for the D-D fuel, could produce energetic protons (3.5 MeV), which will in turn transfer their energy to the fusion species (p, $^{11}$B), increasing their low $T_{in}$ to favorable nuclear reaction cross section values, for the generation of a high-density energetic alphas (2.9 MeV). The energy transfer from the energetic protons and the produced energetic alphas to the fusion species will further contribute to the fast enhancement of the reaction rate and consequently, the p-$^{11}$B medium fusion ignition.

High-power laser facilities may provide the necessary conditions for efficient $\mu$CF, through the re-examination of the fusion process, using specific configurations and fusion fuels. Preliminary experimental studies could be undertaken on muon interaction with high density clusters of deuterium[136,137] or droplets (clusters) of specific composition, such as Ammonia Borane (AB:$H_3BNH_3$) or heavy-(AB) (AB-d6:$D_3BND_3$)[138,139]. Diagnostics development, based

Downloaded from https://www.cambridge.org/core. 19 Nov 2026 at 10:23:14, subject to the Cambridge Core terms of use.

on temporal correlation measurements between the produced neutrons and the alphas will provide significant information on $\mu$CF, using different mixtures of fusion fuels. Numerical results[140], concerning the irradiation of a D-boron mixture in a cavity, by a high-power laser beam, show the production of a significant number of alphas, originating from the interaction of the produced (D+D) energetic protons (3.5 MeV) with boron. These simulations confirm the interest for the use of appropriate mixtures of fusion fuel in the above described $\mu$CF techniques, which could be applied for the fusion ignition of an initial low-temperature p-$^{11}$B medium.

## 5. Conclusions

In summary, this paper presents a comprehensive survey of the current state of research in high-peak-power petawatt-class, laser-driven plasma accelerator production of muons. Analytic formulae provided allow one to estimate the likely electron beam energies using the input parameters of laser pulse energy, pulse duration, peak power, and plasma density. These equations allow one to estimate the likely output of a laser-driven muon source and match well with experiments. Muon yields and spectra depend heavily on the parameters of the electron beam and converter material, but they can be estimated by means of MC as shown in Sec.3 Fig.4 and Sec.3.7 Fig.7 Summaries of the major successful laser-driven muon production experiments conducted worldwide in recent years were presented. From these experimental results, one can ascertain that, with a petawatt class laser of pulse duration between 30 fs and 150 fs, electron bunches of a few GeV and around 100 pC are produced yielding of the order of 1000 muons per shot employing a high-Z converter (like tungsten). Factoring in the high-repetition rates currently achievable with PW lasers (few Hz), LWFA-muon fluxes can exceed cosmic muon fluxes by a considerable factor. Also observed in experiments is that the muon beam is in a forward cone of roughly 30 degrees. From these results we conclude that with near future PW-class lasers operating at 10 Hz, compact laser-driven muon sources (with footprint $\sim$ 50 m$^2$) may become technically feasible. This prospect opens the possibility of a range of applications, also briefly discussed in this paper, with such a pulsed, directed muon source that are not possible with cosmic ray muons. Near-future research in this field should focus on a number of avenues including the increase in electron energy with plasma acceleration to several 10s GeV and charge per bunch of $>$ 1 nC as well as improving the control over and the quality of the muon beam. Further developments in high-peak-power laser technology at high-repetition rates based on direct diode-pumping[81,141,142] will enable compact, efficient accelerators. Equally important will be the development of dedicated muon diagnostics capable of operating in the unique high-background environment of laser-plasma facilities. While mature muon detector technologies already exist for cosmic-ray and high-energy physics applications, their adaptation to pulsed laser-driven sources remains an active area of research. Advances in detector efficiency, background rejection, momentum reconstruction, tracking capability, and high-rate data acquisition will be essential for the full characterization and practical deployment of laser-driven muon sources. With these advances, tunable, compact, cost-effective, directional, and potentially mobile muon sources for applications in fields of high-energy physics, national security and civil engineering should be possible in the next decade.

## Acknowledgement

Lawrence Livermore National Laboratory, ELI Beamlines Facility, University of Maryland, Colorado State University, and Lawrence Berkeley National Laboratory were supported by the Defense Advanced Research Projects Agency (DARPA) under the Muons for Science and Security Program.

Lawrence Livermore National Laboratory wishes to acknowledge that this work was performed under the auspices of the U.S. Department of Energy by Lawrence Livermore National Laboratory under Contract DE-AC52-07NA27344.

Colorado State University is supported by the US Department of Energy, Office of Science, Office of Fusion Energy Science Lasernet US Program, DE-SC0021246.

Queen's University Belfast wishes to acknowledge support from the EPSRC (Grant No: EP/V049186/1) and funding from the EUPRAXIA-PP HORIZON-INFRA-2021-DEV-02 EUR project 101079773.

ELI Beamlines Facility wishes to acknowledge that this work was supported by the National Science Foundation and Czech Science Foundation under NSF-GACR collaborative Grant No. 2206059 from the Czech Science Foundation Grant No. 22-42963L.

## References

1. S. H. Neddermeyer and C. D. Anderson. Note on the nature of cosmic-ray particles. *Phys. Rev.*, 51:884–886, 1937. doi: https://doi.org/10.1103/PhysRev.51.884.
2. G. Charpak, P. J. M. Farley, E. L. Garwin, T. Muller, J. C. Sens, and A. Zichichi. The anomalous magnetic moment of the muon. *Nuovo Cimento*, 37:1241–1363, 1965. doi: https://doi.org/10.1007/BF02783344.
3. T.P. Gorringe and D.W. Hertzog. Precision muon physics. *Progress in Particle and Nuclear Physics*, 84: 73–123, 2015. doi: https://doi.org/10.1016/j.ppnp.2015.06.001.
4. P. Scampoli and A. Ariga. *Cosmic Ray Muography*.

Downloaded from https://www.cambridge.org/core. 19 Nov 2026 at 10:23:14, subject to the Cambridge Core terms of use.

World Scientific, 2023. doi: https://doi.org/10.1142/13102.

5. S. Navas, C. Amsler, T. Gutsche, C. Hanhart, J. J. Hernández-Rey, C. Lourenço, A. Masoni, M. Mikhasenko, R. E. Mitchell, C. Patrignani, C. Schwanda, S. Spanier, G. Venanzoni, C. Z. Yuan, K. Agashe, G. Aielli, B. C. Allanach, J. Alvarez-Muñiz, M. Antonelli, E. C. Aschenauer, D. M. Asner, K. Assamagan, H. Baer, Sw. Banerjee, R. M. Barnett, L. Baudis, C. W. Bauer, J. J. Beatty, J. Beringer, A. Bettini, O. Biebel, K. M. Black, E. Blucher, R. Bonventre, R. A. Briere, A. Buckley, V. D. Burkert, M. A. Bychkov, R. N. Cahn, Z. Cao, M. Carena, G. Casarosa, A. Ceccucci, A. Cerri, R. S. Chivukula, G. Cowan, K. Cranmer, V. Crede, O. Cremonesi, G. D'Ambrosio, T. Damour, D. de Florian, A. de Gouvêa, T. DeGrand, S. Demers, Z. Demiragli, B. A. Dobrescu, M. D'Onofrio, M. Doser, H. K. Dreiner, P. Eerola, U. Egede, S. Eidelman, A. X. El-Khadra, J. Ellis, S. C. Eno, J. Erler, V. V. Ezhela, A. Fava, W. Fetscher, B. D. Fields, A. Freitas, H. Gallagher, T. Gershon, Y. Gershtein, T. Gherghetta, M. C. Gonzalez-Garcia, M. Goodman, C. Grab, A. V. Gritsan, C. Grojean, D. E. Groom, M. Grünewald, A. Gurtu, H. E. Haber, M. Hamel, S. Hashimoto, Y. Hayato, A. Hebecker, S. Heinemeyer, K. Hikasa, J. Hisano, A. Höcker, J. Holder, L. Hsu, J. Huston, T. Hyodo, Al. Ianni, M. Kado, M. Karliner, U. F. Katz, M. Kenzie, V. A. Khoze, S. R. Klein, F. Krauss, M. Kreps, P. Križan, B. Krusche, Y. Kwon, O. Lahav, L. P. Lellouch, J. Lesgourgues, A. R. Liddle, Z. Ligeti, C.-J. Lin, C. Lippmann, T. M. Liss, A. Lister, L. Littenberg, K. S. Lugovsky, S. B. Lugovsky, A. Lusiani, Y. Makida, F. Maltoni, A. V. Manohar, W. J. Marciano, J. Matthews, U.-G. Meißner, I.-A. Melzer-Pellmann, P. Mertsch, D. J. Miller, D. Milstead, K. Mönig, P. Molaro, F. Moortgat, M. Moskovic, N. Nagata, K. Nakamura, M. Narain, P. Nason, A. Nelles, M. Neubert, Y. Nir, H. B. O'Connell, C. A. J. O'Hare, K. A. Olive, J. A. Peacock, E. Pianori, A. Pich, A. Piepke, F. Pietropaolo, A. Pomarol, S. Pordes, S. Profumo, A. Quadt, K. Rabbertz, J. Rademacker, G. Raffelt, M. Ramsey-Musolf, P. Richardson, A. Ringwald, D. J. Robinson, S. Roesler, S. Rolli, A. Romaniouk, L. J Rosenberg, J. L. Rosner, G. Rybka, M. G. Ryskin, R. A. Ryutin, B. Safdi, Y. Sakai, S. Sarkar, F. Sauli, O. Schneider, S. Schönert, K. Scholberg, A. J. Schwartz, J. Schwiening, D. Scott, F. Sefkow, U. Seljak, V. Sharma, S. R. Sharpe, V. Shiltsev, G. Signorelli, M. Silari, F. Simon, T. Sjöstrand, P. Skands, T. Skwarnicki, G. F. Smoot, A. Soffer, M. S. Sozzi, C. Spiering, A. Stahl, Y. Sumino, F. Takahashi, M. Tanabashi, J. Tanaka, M. Taševský, K. Terao, K. Terashi, J. Terning, U. Thoma, R. S. Thorne, L. Tiator, M. Titov, D. R. Tovey, K. Trabelsi, P. Urquijo, G. Valencia, R. Van de Water, N. Varelas, L. Verde, I. Vivarelli, P. Vogel, W. Vogelsang, V. Vorobyev, S. P. Wakely, W. Walkowiak, C. W. Walter, D. Wands, D. H. Weinberg, E. J. Weinberg, N. Wermes, M. White, L. R. Wiencke, S. Willocq, C. L. Woody, R. L. Workman, W.-M. Yao, M. Yokoyama, R. Yoshida, G. Zanderighi, G. P. Zeller, R.-Y. Zhu, S.-L. Zhu, F. Zimmermann, P. A. Zyla, J. Anderson, M. Kramer, P. Schaffner, and W. Zheng. Review of particle physics. *Phys. Rev. D*, 110(3):030001, 2024. doi: https://doi.org/10.1103/PhysRevD.110.030001.

6. Y. Su Tsai. Pair production and bremsstrahlung of charged leptons. *Reviews of Modern Physics*, 46:815–851, 1974. doi: https://doi.org/10.1103/RevModPhys.46.815.

7. G. Dal Maso, A. Gabard, M. Haj Tahar, P.-R. Kettle, K. Kirch, D. Kiselev, A. Koschik, A. Knecht, D. Laube, A. Papa, T. Rauber, D. Reggiani, R. Riccioli, J. Snuverink, V. Talanov, and E. Valetov. Future facilities at psi, the high-intensity muon beams (himb) project. *EPJ Web Conf.*, 282:01012, 2023. doi: https://doi.org/10.1051/epjconf/202328201012.

8. A. D. Hillier, J. S. Lord, K. Ishida, and C. Rogers. Muons at ISIS. *Phil. Trans. Roy. Soc. Lond. A*, 377(2137): 20180064, 2019. doi: https://doi.org/10.1098/rsta.2018.0064.

9. T. Yamazaki. J-PARC muon facility. *PoS*, Muon4Future2023:003, 2024. doi: https://doi.org/10.22323/1.452.0003.

10. G. M. Marshall. Muon beams and facilities at triumf. *Z. Phys. C - Particles and Fields*, 56:S226–S232, 1992. doi: https://doi.org/10.1007/BF02426801.

11. D. Banerjee, J. Bernhard, M. Brugger, N. Charitonidis, V. de Jesus, L. Gatignon, A. Gerbershagen, E. Montbarbon, B. Rae, M. Rosenthal, M.W.U. Van Dijk, B.M. Veit, G.L. D'Alessandro, and S. Cholak. The "physics beyond colliders" projects for the cern m2 beam. *Journal of Physics: Conference Series*, 1350(1):012093, nov 2019. doi: https://doi.org/10.1088/1742-6596/1350/1/012093.

12. F. Metzger. *Studies for current and future high-intensity operation of CERN's secondary M2 beamline*. PhD thesis, Rheinische Friedrich-Wilhelms-Universität Bonn, 9 2024.

13. M. T. Hedges and M. Bloomer. High-power targetry for muon production, 2025. URL https://arxiv.org/abs/2501.10556.

14. B. Madeleine. Analysis of potential target materials for the mu2e production target. In *Proceedings of the Analysis of Potential Target Materials for the Mu2e Production Target*. Fermi National Accelerator Laboratory (FNAL), Batavia, IL (United States), 08 2024. doi: https://doi.org/10.2172/2426573.

15. A. I. Titov, B. Kämpfer, and H. Takabe. Dimuon production by laser-wakefield accelerated electrons. *Phys. Rev. ST Accel. Beams*, 12:111301, 2009. doi: https://doi.org/10.1103/PhysRevSTAB.12.111301.

Downloaded from https://www.cambridge.org/core. 19 Nov 2026 at 10:23:14, subject to the Cambridge Core terms of use.

16. A.W. Chao, K.H. Mess, M. Tigner, and F. Zimmermann. *Handbook of Accelerator Physics and Engineering*. World Scientific, 2nd edition, 2013. doi: https://doi.org/10.1142/8543.
17. P. Muggli, M. Ferrario, J. Osterhoff, and B. Cros. European facilities for advanced accelerators development. *Journal of Instrumentation*, 17, 2022. doi: https://doi.org/10.1088/1748-0221/17/05/T05008.
18. A. Picksley, J. Stackhouse, C. Benedetti, K. Nakamura, H. E. Tsai, R. Li, B. Miao, J. E. Shrock, E. Rockafellow, H.M. Milchberg, C.B. Schroeder, J. van Tilborg, E. Esarey, C.G.R. Geddes, and A.J. Gonsalves. Matched guiding and controlled injection in dark-current-free, 10-gev-class, channel-guided laser-plasma accelerators. *Phys. Rev. Lett.*, 133:255001, 2024. doi: https://doi.org/10.1103/PhysRevLett.133.255001.
19. E. Rockafellow, B. Miao, J. E. Shrock, A. Sloss, M. S. Le, S. W. Hancock, S. Zahedpour, R. C. Hollinger, S. Wang, J. King, P. Zhang, J. Šišma, G. M. Grittani, R. Versaci, D. F. Gordon, G. J. Williams, B. A. Reagan, J. J. Rocca, and H. M. Milchberg. Development of a high charge 10 gev laser electron accelerator. *Phys. Plasmas*, 32(5):053102, 2025. doi: https://doi.org/10.1063/5.0265640.
20. C. Aniculaesei, T. Ha, S. Yoffe, L. Labun, S. Milton, E. McCary, Michael M. Spinks, H.J. Quevedo, O.Z. Labun, R. Sain, A. Hannasch, R. Zgadzaj, I. Pagano, Jose A. F.-A., M.L. Ringuette, E. Gaul, S.V. Luedtke, G. Tiwari, B. Ersfeld, E. Brunetti, H. Ruhl, T. Ditmire, S. Bruce, M.E. Donovan, M.C. Downer, D.A. Jaroszynski, and B.M. Hegelich. The acceleration of a high-charge electron bunch to 10 gev in a 10-cm nanoparticle-assisted wakefield accelerator. *Matter and Radiation at Extremes*, 9(1):014001, 2023. doi: https://doi.org/10.1063/5.0161687.
21. B. Miao, J.E. Shrock, L. Feder, R.C. Hollinger, J. Morrison, R. Nedbailo, A. Picksley, H. Song, S. Wang, J. J. Rocca, and H.M. Milchberg. Multi-GeV Electron Bunches from an All-Optical Laser Wakefield Accelerator. *Phys. Rev. X*, 12(3):031038, 2022. doi: https://doi.org/10.1103/PhysRevX.12.031038.
22. J.D. Ludwig, Kemp A.J. Wilks, S.C., G. J. Williams, N. Lemos, E. Rockafellow, B. Miao, J. E. Shrock, H. M. Milchberg, J.-L. Vay, A. Huebl, R. Lehe, A. Cimmino, R. Versaci, S. V. Bulanov, P. Valenta, V. Tang, and B. A. Reagan. Laser based 100 gev electron acceleration scheme for muon production. *Sci. Rep*, 15:25902, 2025. doi: https://doi.org/10.1038/s41598-025-95440-w.
23. W. Dreesen, J.A. Green, M. Browder, James W., D. Schwellenbach, T. Ditmire, G. Tiwari, and C. Wagner. Detection of petawatt laser-induced muon source for rapid high-z material detection. In *2014 IEEE Nuclear Science Symposium and Medical Imaging Conference (NSS/MIC)*, pages 1–6, 2014. doi: https://doi.org/10.1109/NSSMIC.2014.7431088.
24. F. Zhang, L. Deng, Y. Ge, J. Wen, B. Cui, K. Feng, H. Wang, C. Wu, Z. Pan, H. Liu, Z. Deng, Z. Zhang, L. Chen, D. Yan, Z. Yuan, C. Tian, J. Qian, J. Zhu, and R. Li. Proof-of-principle demonstration of muon production with an ultrashort high-intensity laser. *Nature Physics*, 21:1050–1056, 2025. doi: https://doi.org/10.1038/s41567-025-02872-2.
25. D. Terzani, S. Kisyov, S. Greenberg, L. Le Pottier, M. Mironova, A. Picksley, J. Stackhouse, H.-E. Tsai, R. Li, E. Rockafellow, B. Miao, J. E. Shrock, T. Heim, Maurice G-S, C. Benedetti, J. Valentine, H. M. Milchberg, K. Nakamura, A. J. Gonsalves, J. van Tilborg, C. B. Schroeder, E. Esarey, and C. G. R. Geddes. Measurement of directional muon beams generated at the berkeley lab laser accelerator. *Phys. Rev. Accel. Beams*, 28:103401, 2025. doi: https://doi.org/10.1103/kxjr-h7zs.
26. L. Calvin, E. Gerstmayr, C. Arran, L. Tudor, T. Foster, B. Bergmann, D. Doria, B. Kettle, H. Maguire, V. Malka, P. Manek, S. P. D. Mangles, P. McKenna, R. E. Mihai, C. Ridgers, J. Sarma, P. Smolyanskiy, R. Wilson, R. M. Deas, and G. Sarri. Experimental evidence of muon production from a laser-wakefield accelerator. *Plasma Physics and Controlled Fusion*, 68:035015, 2026. doi: https://doi.org/10.1088/1361-6587/ae4d05.
27. T. Tajima and J. M. Dawson. Laser electron accelerator. *Phys. Rev. Lett.*, 43:267–270, 1979. doi: https://doi.org/10.1103/PhysRevLett.43.267.
28. D. Strickland and G. Mourou. Compression of amplified chirped optical pulses. *Optics Communications*, 56(3):219–221, 1985. doi: https://doi.org/10.1016/0030-4018(85)90120-8.
29. S.P D. Mangles, C.D. Murphy, Z. Najmudin, A.G.R. Thomas, J.L. Collier, A.E. Dangor, E.J. Divall, P.S. Foster, J.G. Gallacher, C.J. Hooker, D.A. Jaroszynski, A.J. Langley, W.B. Mori, P.A. Norreys, F.S. Tsung, R. Viskup, B.R. Walton, and K. Krushelnick. Monoenergetic beams of relativistic electrons from intense laser-plasma interactions. *Nature*, 431:535–538, 2004. doi: https://doi.org/10.1038/nature02939.
30. C.G.R. Geddes, C. Toth, J. van Tilborg, E. Esarey, C.B. Schroeder, D. Bruhwiler, C. Nieter, J. Cary, and W.P. Leemans. High-quality electron beams from a laser wakefield accelerator using plasma-channel guiding. *Nature*, 431:538–541, 2004. doi: https://doi.org/10.1038/nature02900.
31. J. Faure, Y. Glinec, A. Pukhov, S. Kiselev, S. Gordienko, E. Lefebvre, J. P. Rousseau, F. Burgy, and V. Malka. A laser-plasma accelerator producing monoenergetic electron beams. *Nature*, 431:541–544, 2004. doi: https://doi.org/10.1038/nature02963.
32. E. Esarey, C.B. Schroeder, and W.P. Leemans. Physics of laser-driven plasma-based electron accelerators. *Rev. Mod. Phys.*, 81:1229–1285, 2009. doi: https://doi.org/10.

Downloaded from https://www.cambridge.org/core. 19 Nov 2026 at 10:23:14, subject to the Cambridge Core terms of use.

1103/RevModPhys.81.1229.
33. S.V. Bulanov, I.N. Inovenkov, V.I. Kirsanov, N.M. Naumova, and A.S. Sakharov. Ultra fast depletion of ultra-short and relativistically strong laser pulses in an underdense plasma. *Physics of Fluids B*, 4:1935, 1992.
34. C. McGuffey, A.G.R. Thomas, W. Schumaker, T. Matsuoka, V. Chvykov, F.J. Dollar, G. Kalintchenko, V. Yanovsky, A. Maksimchuk, K. Krushelnick, V. Yu. Bychenkov, I.V. Glazyrin, and A. V. Karpeev. Ionization induced trapping in a laser wakefield accelerator. *Phys. Rev. Lett.*, 104:025004, 2010. doi: https://doi.org/10.1103/PhysRevLett.104.025004.
35. A. Pak, K.A. Marsh, S.F. Martins, W. Lu, W.B. Mori, and C. Joshi. Injection and trapping of tunnel-ionized electrons into laser-produced wakes. *Phys. Rev. Lett.*, 104:025003, 2010. doi: https://doi.org/10.1103/PhysRevLett.104.025003.
36. J. Faure, C. Rechatin, A. Norlin, A. Lifschitz, Y. Glinec, and V. Malka. Controlled injection and acceleration of electrons in plasma wakefields by colliding laser pulses. *Nature*, 444:737–739, 2006. doi: https://doi.org/10.1038/nature05393.
37. S. V. Bulanov, N. M. Naumova, F. Pegoraro, and J.-I. Sakai. Particle injection into the acceleration phase of the wake field behind the laser pulse. *Phys. Rev. E*, 58:5257, 1998.
38. A. S. Krass. Photoproduction of muon pairs. *Phys. Rev.*, 138:B1268–B1273, 1965. doi: https://doi.org/10.1103/PhysRev.138.B1268.
39. W. Lu, M. Tzoufras, C. Joshi, F.S. Tsung, W.B. Mori, J. Vieira, R.A. Fonseca, and L. O. Silva. Generating multi-gev electron bunches using single stage laser wakefield acceleration in a 3d nonlinear regime. *Phys. Rev. ST Accel. Beams*, 10:061301, Jun 2007. doi: https://doi.org/10.1103/PhysRevSTAB.10.061301.
40. S.V. Bulanov, T.Z. Esirkepov, Y. Hayashi, H. Kiriyama, J.K. Koga, H. Kotaki, M. Mori, and M. Kando. On some theoretical problems of laser wake-field accelerators. *Journal of Plasma Physics*, 82(3):905820308, 2016. doi: https://doi.org/10.1017/S0022377816000623.
41. P. Valenta, T.Z. Esirkepov, J. D. Ludwig, S. C. Wilks, and S. V. Bulanov. Bayesian optimization of electron energy from laser wakefield accelerators. *Phys. Rev. Accel. Beams*, 28:094601, 2025. doi: https://doi.org/10.1103/knh7-hbr3.
42. P. Valenta and S.V. Bulanov. Optimized scaling for reaching maximum electron energy from laser wakefield accelerator. In Stepan S. Bulanov, Gabriele M. Grittani, and Charlotte A. J. Palmer, editors, *Laser Acceleration of Electrons, Protons, and Ions VIII*, volume 13534, page 1353406. International Society for Optics and Photonics, SPIE, 2025. doi: https://doi.org/10.1117/12.3058376.
43. A. Pukhov and J. Meyer-ter Vehn. Laser wake field acceleration: the highly non-linear broken-wave regime. *Appl. Phys. B*, 74:355, 2003. doi: https://doi.org/10.1007/s003400200795.
44. H. Hora. Theory of relativistic self-focusing of laser radiation in plasmas. *J. Opt. Soc. Am.*, 65(8):882–886, Aug 1975. doi: https://doi.org/10.1364/JOSA.65.000882.
45. J.E. Shrock, B. Miao, L. Feder, and H.M. Milchberg. Meter-scale plasma waveguides for multi-gev laser wakefield acceleration. *Phys. Plasmas*, 29(7):073101, 2022. doi: https://doi.org/10.1063/5.0097214.
46. P.B. Corkum, N.H. Burnett, and F. Brunel. Above-threshold ionization in the long-wavelength limit. *Phys. Rev. Lett.*, 62:1259–1262, 1989. doi: https://doi.org/10.1103/PhysRevLett.62.1259.
47. N. Lemos, T. Grismayer, L. Cardoso, G. Figueira, R. Issac, D.A. Jaroszynski, and J.M. Dias. Plasma expansion into a waveguide created by a linearly polarized femtosecond laser pulse. *Physics of Plasmas*, 20(6):063102, 06 2013. ISSN 1070-664X. doi: https://doi.org/10.1063/1.4810797.
48. R.J. Shalloo, C. Arran, L. Corner, J. Holloway, J. Jonnerby, R. Walczak, H. M. Milchberg, and S. M. Hooker. Hydrodynamic optical-field-ionized plasma channels. *Phys. Rev. E*, 97:053203, 2018. doi: https://doi.org/10.1103/PhysRevE.97.053203.
49. B. Miao, L. Feder, J.E. Shrock, A. Goffin, and H.M. Milchberg. Optical guiding in meter-scale plasma waveguides. *Phys. Rev. Lett.*, 125:074801, Aug 2020. doi: https://doi.org/10.1103/PhysRevLett.125.074801.
50. L. Feder, B. Miao, J. E. Shrock, A. Goffin, and H. M. Milchberg. Self-waveguiding of relativistic laser pulses in neutral gas channels. *Phys. Rev. Res.*, 2:043173, 2020. doi: https://doi.org/10.1103/PhysRevResearch.2.043173.
51. A. Morozov, A. Goltsov, Q. Chen, M. Scully, and S. Suckewer. Ionization assisted self-guiding of femtosecond laser pulses. *Physics of Plasmas*, 25(5):053110, 05 2018. ISSN 1070-664X. doi: https://doi.org/10.1063/1.5021795.
52. A. Picksley, A. Alejo, R.J. Shalloo, C. Arran, A. von Boetticher, L. Corner, J.A. Holloway, J. Jonnerby, O. Jakobsson, C. Thornton, R. Walczak, and S.M. Hooker. Meter-scale conditioned hydrodynamic optical-field-ionized plasma channels. *Phys. Rev. E*, 102:053201, 2020. doi: https://doi.org/10.1103/PhysRevE.102.053201.
53. B. Miao, J.E. Shrock, E. Rockafellow, A.J. Sloss, and H.M. Milchberg. Meter-scale supersonic gas jets for multi-gev laser-plasma accelerators. *Review of Scientific Instruments*, 96(4):043003, 2025. doi: https://doi.org/10.1063/5.0248959.
54. J. Šišma, M. Nevrkla, F. Vitha, S. Lorenz, I. Zymak, A. Špádová, A. Kollárová, M. Jech, A. Jančárek, D. Peceli, C. M. Lazzarini, Leonardo V. N. Goncalves, G. M. Grittani, S. V. Bulanov, J. E. Shrock, E. Rockafellow, A. J. Sloss, B. Miao, S. W. Hancock, and H. M.

Downloaded from https://www.cambridge.org/core. 19 Nov 2026 at 10:23:14, subject to the Cambridge Core terms of use.

Milchberg. High-repetition-rate, all-reflective optical guiding and electron acceleration in helium using an off-axis axicon. *High Power Laser Science and Engineering*, page 1–15, 2026. doi: https://doi.org/10.1017/hpl.2026.10154.

55. C. Radier, O. Chalus, M. Charbonneau, G. Deschamps S. Thambirajah, S. David, J. Barbe, E. Etter, G. Matras, S. Ricaud, V. Leroux, C. Richard, F. Lureau, A. Baleanu, R. Banici, A. Gradinariu, C. Caldararu, C. Capiteanu, A. Naziru, B. Diaconescu, V. Iancu, R. Dabu, D. Ursescu, I. Dancus, C. A. Ur, K. A. Tanaka, and N. V. Zamfir. 10 pw peak power femtosecond laser pulses at eli-np. *High Power Laser Science and Engineering*, 10:e21, 2022. doi: https://doi.org/10.1017/hpl.2022.11.
56. E. Gaul, G. Chériaux, R. Antipenkov, F. Batysta, T. Borger, G. Friedman, J.T. Greene, D. Hammond, J. Heisler, D. Hidinger, A. Jochmann, M. Kepler, A. Kissinger, D. Kramer, J.C. Lagron, A. Meadows, B. Rus, P. Trojek, S. Vyhlídka, and T. Ditmire. Hybrid opcpa/glass 10 pw laser at 1 shot a minute. In *Conference on Lasers and Electro-Optics*, page STu3M.2. Optica Publishing Group, 2018. doi: https://doi.org/10.1364/CLEO_SI.2018.STu3M.2.
57. Z. Li, Y. Leng, and R. Li. Further development of the short-pulse petawatt laser: Trends, technologies, and bottlenecks. *Laser & Photonics Reviews*, 17(1):2100705, 2023. doi: https://doi.org/10.1002/lpor.202100705.
58. C. N. Danson, C. Haefner, J. Bromage, T. Butcher, J.-C. F. Chanteloup, E. A. Chowdhury, A. Galvanauskas, L. A. Gizzi, J. Hein, D. I. Hillier, N. W. Hopps, Y. Kato, E. A. Khazanov, R. Kodama, G. Korn, R. Li, Y. Li, J. Limpert, J. Ma, C. Hee Nam, D. Neely, D. Papadopoulos, R. R. Penman, L. Qian, J. J. Rocca, A. A. Shaykin, C. W. Siders, C. Spindloe, S. Szatmári, R. M. G. M. Trines, J. Zhu, P. Zhu, and J. D. Zuegel. Petawatt and exawatt class lasers worldwide. *High Power Laser Science and Engineering*, 7:e54, 2019. doi: https://doi.org/10.1017/hpl.2019.36.
59. Z. hang, F. Wu, J. Hu, X. Yang, J. Gui, P. Ji, X. Liu, C. Wang, Y. Liu, X. Lu, Y. Xu, Y. Leng, R. Li, and Y. Xu. The $1\ \mathrm{PW}/0.1\ \mathrm{Hz}$ laser beamline in sulf facility. *High Power Laser Science and Engineering*, 8:e4, 2020. doi: https://doi.org/10.1017/hpl.2020.3.
60. J.Y. Yoo J.W. Yoon C.W. Lee J.M. Yang Y.J. Son Y.H. Jang S.K. Lee J.H. Sung, H.W. Lee and C.H. Nam. 4.2 pw, 20 fs ti:sapphire laser at 0.1 hz. *Opt. Lett.*, 42(11):2058–2061, 2017. doi: https://doi.org/10.1364/OL.42.002058.
61. K. Põder, J. C. Wood, N. C. Lopes, J. M. Cole, S. Alatabi, M. P. Backhouse, P. S. Foster, A. J. Hughes, C. Kamperidis, O. Kononenko, S. P. D. Mangles, C. A. J. Palmer, D. Rusby, A. Sahai, G. Sarri, D. R. Symes, J. R. Warwick, and Z. Najmudin. Multi-gev electron acceleration in wakefields strongly driven by oversized laser spots. *Phys. Rev. Lett.*, 132:195001, 2024. doi: https://doi.org/10.1103/PhysRevLett.132.195001.
62. M. O. Cernaianu, P. Ghenuche, F. Rotaru, L. Tudor, O. Chalus, C. Gheorghiu, D. C. Popescu, M. Gugiu, S. Balascuta, A. Magureanu, M. Tataru, V. Horny, B. Corobean, I. Dancus, A. Alincutei, T. Asavei, B. Diaconescu, L. Dinca, D. B. Dreghici, D. G. Ghita, C. Jalba, V. Leca, A. M. Lupu, V. Nastasa, F. Negoita, M. Patrascoiu, F. Schimbeschi, D. Stutman, C. Ticos, D. Ursescu, A. Arefiev, P. Tomassini, V. Malka, S. Gales, K. A. Tanaka, C. A. Ur, and D. Doria. Commissioning of the 1 pw experimental area at eli-np using a short focal parabolic mirror for proton acceleration. *Matter and Radiation at Extremes*, 10(2):027204, 03 2025. doi: https://doi.org/10.1063/5.0241077.
63. C.A. Ur, D. Balabanski, M. Cernăianu, D. Doria, P. Ghenuche, A. Kusoglu, N. Safca, P.-A. Söderstrom, and D. Stutman. Extreme light infrastructure - nuclear physics: first results. *Eur. Phys. J. A*, 61:248, 2025. doi: https://doi.org/10.1140/epja/s10050-025-01713-3.
64. G. Battistoni, T. Boehlen, F. Cerutti, P. W. Chin, L. S. Esposito, A. Fassò, A. Ferrari, A. Lechner, A. Empl, A. Mairani, A. Mereghetti, P. G. Ortega, J. Ranft, S. Roesler, P. R. Sala, V. Vlachoudis, and G. Smirnov. Overview of the fluka code. *Annals of Nuclear Energy*, 82:10–18, 2015. doi: https://doi.org/10.1016/j.anucene.2014.11.007.
65. C. Ahdida, D. Bozzato, D. Calzolari, F. Cerutti, N. Charitonidis, A. Cimmino, A. Coronetti, G. L. D'Alessandro, A. Donadon Servelle, L. S. Esposito, R. Froeschl, R. García Alía, A. Gerbershagen, S. Gilardoni, D. Horváth, G. Hugo, A. Infantino, V. Kouskoura, A. Lechner, B. Lefebvre, G. Lerner, M. Magistris, A. Manousos, G. Moryc, F. Ogallar Ruiz, F. Pozzi, D. Prelipcean, S. Roesler, R. Rossi, M. Sabaté Gilarte, F. Salvat Pujol, P. Schoofs, V. Stránský, C. Theis, A. Tsinganis, R. Versaci, V. Vlachoudis, A. Waets, and M. Widorski. New capabilities of the fluka multi-purpose code. *Frontiers in Physics*, 9:788253, 2022. doi: https://doi.org/10.3389/fphy.2021.788253.
66. A. Donadon, G. Hugo, C. Theis, and V. Vlachoudis. Flair3 – recasting simulation experiences with the advanced interface for fluka and other monte carlo codes. *EPJ Web of Conferences*, 302:11005, 2024. doi: https://doi.org/10.1051/epjconf/202430211005.
67. A. Fasso, A. Ferrari, N. V. Mokhov, S. E. Mueller, W. R. Nelson, S. Roesler, T. Sanami, S. I. Striganov, and R. Versaci. Update on the code intercomparison and benchmark for muon fluence and absorbed dose induced by an 18-gev electron beam after massive iron shielding. In *13th Meeting of the task- force on Shielding aspects of Accelerators, Targets and Irradiation Facilities*, 12 2016.
68. Y. Wang and Y. Yu. Multigap resistive plate chambers for time of flight applications. *Appl. Sci.*, 11:111, 2021. doi: https://doi.org/10.3390/app11010111.

Downloaded from https://www.cambridge.org/core. 19 Nov 2026 at 10:23:14, subject to the Cambridge Core terms of use.

69. J. Bortfeldt, F. Brunbauer, C. David, D. Desforge, G. Fanourakis, J. Franchi, M. Gallinaro, I. Giomataris, D. González-Díaz, T. Gustavsson, C. Guyot, F.J. Iguaz, M. Kebbiri, P. Legou, J. Liu, M. Lupberger, O. Maillard, I. Manthos, H. Müller, V. Niaouris, E. Oliveri, T. Papaevangelou, K. Paraschou, M. Pomorski, B. Qi, F. Resnati, L. Ropelewski, D. Sampsonidis, T. Schneider, P. Schwemling, L. Sohl, M. van Stenis, P. Thuiner, Y. Tsipolitis, S.E. Tzamarias, R. Veenhof, X. Wang, S. White, Z. Zhang, and Y. Zhou. Picosec: Charged particle timing at sub-25 picosecond precision with a micromegas based detector. *Nuclear Instruments and Methods in Physics Research Section A: Accelerators, Spectrometers, Detectors and Associated Equipment*, 903: 317–325, 2018. doi: https://doi.org/10.1016/j.nima.2018.04.033.

70. E. W. Gaul, M. Martinez, J. B., A. Jochmann, M. Ringuette, D. Hammond, T. Borger, R. Escamilla, S. Douglas, W. Henderson, G. Dyer, A. Erlandson, R. Cross, J. Caird, C. Ebbers, and T. Ditmire. Demonstration of a 1.1 petawatt laser based on a hybrid optical parametric chirped pulse amplification/mixed nd:glass amplifier. *Appl. Opt.*, 49(9):1676–1681, 2010. doi: https://doi.org/10.1364/AO.49.001676.

71. X. Wang, R. Zgadzaj, S. A. Yi, V. Khudik, W. Henderson, N. Fazel, Y.-Y. Chang, R. Korzekwa, H.-E. Tsai, C.-H. Pai, Z. Li, E. Gaul, M. Martinez, G. Dyer, H. Quevedo, A. Bernstein, M. Donovan, G. Shvets, T. Ditmire, and M. C. Downer. Self-injected petawatt laser-driven plasma electron acceleration in $10^17$ $cm^3$ plasma. *Journal of Plasma Physics*, 78(4):413–419, 2012. doi: https://doi.org/10.1017/S002237781200030X.

72. X. Wang, R. Zgadzaj, N. Fazel, S. A. Yi, X. Zhang, W. Henderson, Y.-Y. Chang, R. Korzekwa, H.-E. Tsai, C.-H. Pai, Z. Li, H. Quevedo, G. Dyer, E. Gaul, M. Martinez, A. Bernstein, T. Borger, M. Spinks, M. Donovan, S. Y. Kalmykov, V. Khudik, G. Shvets, T. Ditmire, and M. C. Downer. Petawatt-laser-driven wakefield acceleration of electrons to 2 gev in 1017 cm3 plasma. *AIP Conference Proceedings*, 1507(1):341–344, 2012. doi: https://doi.org/10.1063/1.4773719.

73. X. Wang, R. Zgadzaj, N. Fazel, Z. Li, W. Henderson, Y.-Y. Chang, R. Korzekwa, S. A. Yi, V. Khudik, X. Zhang, H-E Tsai, C.-H Pai, H. Quevedo, G. Dyer, E. Gaul, M. Martinez, A. Bernstein, T. Borger, M. Spinks, M. Donovan, G. Shvets, T. Ditmire, and M. C. Downer. Gev electrons and high brightness betatron x-rays from petawatt-laser-driven plasma accelerators. In *CLEO: 2014*, page FM1B.2. Optica Publishing Group, 2014. doi: https://doi.org/10.1364/CLEO_QELS.2014.FM1B.2.

74. J. M. Shaw, A. C. Bernstein, A. Hannasch, M. LaBerge, Y.-Y. Chang, K. Weichman, J. Welch, R. Zgadzaj, W. Henderson, H.-E. Tsai, N. Fazel, X. Wang, C. Wagner, M. Donovan, G. Dyer, E. Gaul, J. Gordon, M. Martinez, M. Spinks, T. Toncian, T. Ditmire, and M. C. Downer. Generation of tens-of-mev photons by compton backscatter from laser-plasma-accelerated gev electrons. *AIP Conference Proceedings*, 1812(1):100012, 2017. doi: https://doi.org/10.1063/1.4975910.

75. S. Agostinelli, J. Allison, K. Amako, J. Apostolakis, H. Araujo, P. Arce, M. Asai, D. Axen, S. Banerjee, G. Barrand, F. Behner, L. Bellagamba, J. Boudreau, L. Broglia, A. Brunengo, H. Burkhardt, S. Chauvie, J. Chuma, R. Chytracek, G. Cooperman, G. Cosmo, P. Degtyarenko, A. Dell'Acqua, G. Depaola, D. Dietrich, R. Enami, A. Feliciello, C. Ferguson, H. Fesefeldt, G. Folger, F. Foppiano, A. Forti, S. Garelli, S. Giani, R. Giannitrapani, D. Gibin, J.J. Gómez Cadenas, I. González, G. Gracia Abril, G. Greeniaus, W. Greiner, V. Grichine, A. Grossheim, S. Guatelli, P. Gumplinger, R. Hamatsu, K. Hashimoto, H. Hasui, A. Heikkinen, A. Howard, V. Ivanchenko, A. Johnson, F.W. Jones, J. Kallenbach, N. Kanaya, M. Kawabata, Y. Kawabata, M. Kawaguti, S. Kelner, P. Kent, A. Kimura, T. Kodama, R. Kokoulin, M. Kossov, H. Kurashige, E. Lamanna, T. Lampén, V. Lara, V. Lefebure, F. Lei, M. Liendl, W. Lockman, F. Longo, S. Magni, M. Maire, E. Medernach, K. Minamimoto, P. Mora de Freitas, Y. Morita, K. Murakami, M. Nagamatu, R. Nartallo, P. Nieminen, T. Nishimura, K. Ohtsubo, M. Okamura, S. O'Neale, Y. Oohata, K. Paech, J. Perl, A. Pfeiffer, M.G. Pia, F. Ranjard, A. Rybin, S. Sadilov, E. Di Salvo, G. Santin, T. Sasaki, N. Savvas, Y. Sawada, S. Scherer, S. Sei, V. Sirotenko, D. Smith, N. Starkov, H. Stoecker, J. Sulkimo, M. Takahata, S. Tanaka, E. Tcherniaev, E. Safai Tehrani, M. Tropeano, P. Truscott, H. Uno, L. Urban, P. Urban, M. Verderi, A. Walkden, W. Wander, H. Weber, J.P. Wellisch, T. Wenaus, D.C. Williams, D. Wright, T. Yamada, H. Yoshida, and D. Zschiesche. Geant4—a simulation toolkit. *Nuclear Instruments and Methods in Physics Research Section A: Accelerators, Spectrometers, Detectors and Associated Equipment*, 506(3):250–303, 2003. doi: https://doi.org/10.1016/S0168-9002(03)01368-8.

76. W. Dreesen, J. A. Green, M. Browder, J. Wood, D. Schwellenbach, T. Ditmire, G. Tiwari, and C. Wagner. Detection of petawatt laser-induced muon source for rapid high-z material detection. In *2014 IEEE Nuclear Science Symposium and Medical Imaging Conference (NSS/MIC)*, pages 1–6, 2014. doi: https://doi.org/10.1109/NSSMIC.2014.7431088.

77. F. Zhang, B. Li, B. Zhang, W. Hong, and Y. Gu. A new method on diagnostics of muons produced by a short pulse laser. *High Power Laser Science and Engineering*, 5, 07 2017. doi: https://doi.org/10.1017/hpl.2017.15.

78. Z. Gan, L. Yu, C. Wang, Y. Liu, Y. Xu, W. Li, S. Li, L. Yu, W. Xinliang, X. Liu, C. Junchi, Y. Peng, L. Xu, B. Yao, X. Zhang, L. Chen, Y. Tang, X. Wang, D. Yin, and

Downloaded from https://www.cambridge.org/core. 19 Nov 2026 at 10:23:14, subject to the Cambridge Core terms of use.

Z. Xu. The shanghai superintense ultrafast laser facility (sulf) project. *Topics in Applied Physics*, pages 199–217, 2021. doi: https://doi.org/10.1007/978-3-030-75089-3_10.

79. J. Allison, K. Amako, J. Apostolakis, H. Araujo, P. Arce Dubois, M. Asai, G. Barrand, R. Capra, S. Chauvie, R. Chytracek, G.A.P. Cirrone, G. Cooperman, G. Cosmo, G. Cuttone, G.G. Daquino, M. Donszelmann, M. Dressel, G. Folger, F. Foppiano, J. Generowicz, V. Grichine, S. Guatelli, P. Gumplinger, A. Heikkinen, I. Hrivnacova, A. Howard, S. Incerti, V. Ivanchenko, T. Johnson, F. Jones, T. Koi, R. Kokoulin, M. Kossov, H. Kurashige, V. Lara, S. Larsson, F. Lei, O. Link, F. Longo, M. Maire, A. Mantero, B. Mascialino, I. McLaren, P. Mendez Lorenzo, K. Minamimoto, K. Murakami, P. Nieminen, L. Pandola, S. Parlati, L. Peralta, J. Perl, A. Pfeiffer, M.G. Pia, A. Ribon, P. Rodrigues, G. Russo, S. Sadilov, G. Santin, T. Sasaki, D. Smith, N. Starkov, S. Tanaka, E. Tcherniaev, B. Tome, A. Trindade, P. Truscott, L. Urban, M. Verderi, A. Walkden, J.P. Wellisch, D.C. Williams, D. Wright, and H. Yoshida. Geant4 developments and applications. *IEEE Transactions on Nuclear Science*, 53(1):270–278, 2006. doi: https://doi.org/10.1109/TNS.2006.869826.
80. J. Allison, K. Amako, J. Apostolakis, P. Arce, M. Asai, T. Aso, E. Bagli, A. Bagulya, S. Banerjee, G. Barrand, B.R. Beck, A.G. Bogdanov, D. Brandt, J.M.C. Brown, H. Burkhardt, Ph. Canal, D. Cano-Ott, S. Chauvie, K. Cho, G.A.P. Cirrone, G. Cooperman, M.A. Cortés-Giraldo, G. Cosmo, G. Cuttone, G. Depaola, L. Desorgher, X. Dong, A. Dotti, V.D. Elvira, G. Folger, Z. Francis, A. Galoyan, L. Garnier, M. Gayer, K.L. Genser, V.M. Grichine, S. Guatelli, P. Guèye, P. Gumplinger, A.S. Howard, I. Hřivnáčová, S. Hwang, S. Incerti, A. Ivanchenko, V.N. Ivanchenko, F.W. Jones, S.Y. Jun, P. Kaitaniemi, N. Karakatsanis, M. Karamitros, M. Kelsey, A. Kimura, T. Koi, H. Kurashige, A. Lechner, S.B. Lee, F. Longo, M. Maire, D. Mancusi, A. Mantero, E. Mendoza, B. Morgan, K. Murakami, T. Nikitina, L. Pandola, P. Paprocki, J. Perl, I. Petrović, M.G. Pia, W. Pokorski, J.M. Quesada, M. Raine, M.A. Reis, A. Ribon, A. Ristić Fira, F. Romano, G. Russo, G. Santin, T. Sasaki, D. Sawkey, J.I. Shin, I.I. Strakovsky, A. Taborda, S. Tanaka, B. Tomé, T. Toshito, H.N. Tran, P.R. Truscott, L. Urban, V. Uzhinsky, J.M. Verbeke, M. Verderi, B.L. Wendt, H. Wenzel, D.H. Wright, D.M. Wright, T. Yamashita, J. Yarba, and H. Yoshida. Recent developments in geant4. *Nuclear Instruments and Methods in Physics Research Section A: Accelerators, Spectrometers, Detectors and Associated Equipment*, 835: 186–225, 2016. doi: https://doi.org/10.1016/j.nima.2016.06.125.
81. I. Tamer, Z. Hubka, L. Kiani, J. Owens, A. Church, F. Batysta, T. Galvin, D. Willard, A. Yandow, J. Galbraith, D. Alessi, C. Harthcock, B. Hickman, C. Jackson, J. Nissen, S. Tardiff, H. Nguyen, E. Sistrunk, T. Spinka, and B. A. Reagan. Demonstration of a 1 tw peak power, joule-level ultrashort tm:ylf laser. *Opt. Lett.*, 49(6):1583–1586, 2024. doi: https://doi.org/10.1364/OL.519542.
82. Y. Wang, S. Wang, A. Rockwood, B.M. Luther, R. Hollinger, A. Curtis, C. Calvi, C.S. Menoni, and J.J. Rocca. 0.85pw laser operation at 3.3 hz and high-contrast ultrahigh-intensity $\lambda = 400$ nm second-harmonic beamline. *Opt. Lett.*, 42(19):3828–3831, 2017. doi: https://doi.org/10.1364/OL.42.003828.
83. J. E. Shrock, E. Rockafellow, B. Miao, M. Le, R. C. Hollinger, S. Wang, A. J. Gonsalves, A. Picksley, J. J. Rocca, and H. M. Milchberg. Guided mode evolution and ionization injection in meter-scale multi-gev laser wakefield accelerators. *Phys. Rev. Lett.*, 133(4):045002, 2024. doi: https://doi.org/10.1103/PhysRevLett.133.045002.
84. E. Rockafellow, J. E. Shrock, B. Miao, A. J. Sloss, M. S. Le, S. W. Hancock, S. Zahedpour, R. C. Hollinger, S. Wang, J. King, P. Zhang, J. Šišma, G. M. Grittani, R. Versaci, D. F. Gordon, G. J. Williams, Brendan A. R., J. J. Rocca, and H. M. Milchberg. High charge laser acceleration of electrons to 10 gev. *Nuclear Instruments and Methods in Physics Research Section A: Accelerators, Spectrometers, Detectors and Associated Equipment*, 1077:170586, 2025. doi: https://doi.org/10.1016/j.nima.2025.170586.
85. S. Gordienko and A. Pukhov. Scalings for ultrarelativistic laser plasmas and quasimonoenergetic electrons. *Physics of Plasmas*, 12(4):043109, 2005. doi: https://doi.org/10.1063/1.1884126.
86. X. Zhu, Min Chen, S. Weng, T. Yu, W. Wang, F. He, Z. Sheng, P. McKenna, D. A. Jaroszynski, and J. Zhang. Extremely brilliant gev -rays from a two-stage laser-plasma accelerator. *Science Advances*, 6(22):eaaz7240, 2020. doi: https://doi.org/10.1126/sciadv.aaz7240.
87. L. Calvin, P. Tomassini, D. Doria, D. Martello, R. M. Deas, and G. Sarri. Laser-driven muon production for material inspection and imaging. *Frontiers in Physics*, 11, 2023. doi: https://doi.org/10.3389/fphy.2023.1177486.
88. P. Mason, N. Stuart, J. Phillips, R. Heathcote, S. Buck, A. Wojtusiak, M. Galimberti, T. de Faria Pinto, S. Hawkes, S. Tomlinson, R. Pattathil, T. Butcher, C. Hernandez-Gomez, and J. Collier. Progress on laser development at the extreme photonics applications centre. In *2023 Conference on Lasers and Electro-Optics Europe European Quantum Electronics Conference (CLEO/Europe-EQEC)*, pages 1–1, 2023. doi: https://doi.org/10.1109/CLEO/Europe-EQEC57999.2023.10232104.
89. R. W. Assmann, M. K. Weikum, T. Akhter, D. Alesini, A. S. Alexandrova, M. P. Anania, N. E. Andreev, I. Andriyash, M. Artioli, A. Aschikhin, T. Audet, A. Bacci, I. F.

Downloaded from https://www.cambridge.org/core. 19 Nov 2026 at 10:23:14, subject to the Cambridge Core terms of use.

Barna, S. Bartocci, A. Bayramian, A. Beaton, A. Beck, M. Bellaveglia, A. Beluze, A. Bernhard, A. Biagioni, S. Bielawski, F. G. Bisesto, A. Bonatto, L. Boulton, F. Brandi, R. Brinkmann, F. Briquez, F. Brottier, E. Brundermann, M. Buscher, B. Buonomo, M. H. Bussmann, G. Bussolino, P. Campana, S. Cantarella, K. Cassou, A. Chance, M. Chen, E. Chiadroni, A. Cianchi, F. Cioeta, J. A. Clarke, J. M. Cole, G. Costa, M.-E. Couprie, J. Cowley, M. Croia, B. Cros, P. A. Crump, R. D'Arcy, G. Dattoli, Dotto A. Del, N. Delerue, M. Del Franco, P. Delinikolas, S. De Nicola, J. M. Dias, D. Di Giovenale, M. Diomede, E. Di Pasquale, G. Di Pirro, G. Di Raddo, U. Dorda, A. C. Erlandson, K. Ertel, A. Esposito, F. Falcoz, A. Falone, R. Fedele, A. Ferran Pousa, M. Ferrario, F. Filippi, J. Fils, G. Fiore, R. Fiorito, R. A. Fonseca, G. Franzini, M. Galimberti, A. Gallo, T. C. Galvin, A. Ghaith, A. Ghigo, D. Giove, A. Giribono, L. A. Gizzi, F. J. Grüner, A. F. Habib, C. Haefner, T. Heinemann, A. Helm, B. Hidding, B. J. Holzer, S. M. Hooker, T. Hosokai, M. Hübner, M. Ibison, S. Incremona, A. Irman, F. Iungo, F. J. Jafarinia, O. Jakobsson, D. A. Jaroszynski, S. Jaster-Merz, C. Joshi, M. Kaluza, M. Kando, O. S. Karger, S. Karsch, E. Khazanov, D. Khikhlukha, M. Kirchen, G. Kirwan, C. Kitégi, A. Knetsch, D. Kocon, P. Koester, O. S. Kononenko, G. Korn, I. Kostyukov, K. O. Kruchinin, L. Labate, C. Le Blanc, C. Lechner, P. Lee, W. Leemans, A. Lehrach, X. Li, Y. Li, V. Libov, A. Lifschitz, C. A. Lindstrøm, V. Litvinenko, W. Lu, O. Lundh, A. R. Maier, V. Malka, G. G. Manahan, S. P. D. Mangles, A. Marcelli, B. Marchetti, O. Marcouillé, A. Marocchino, F. Marteau, A. Martinez de la Ossa, J. L. Martins, P. D. Mason, F. Massimo, F. Mathieu, G. Maynard, Z. Mazzotta, S. Mironov, A. Y. Molodozhentsev, S. Morante, A. Mosnier, A. Mostacci, A. S. Müller, C. D. Murphy, Z. Najmudin, P. A. P. Nghiem, F. Nguyen, P. Niknejadi, A. Nutter, J. Osterhoff, D. Oumbarek Espinos, J. L. Paillard, D. N. Papadopoulos, B. Patrizi, R. Pattathil, L. Pellegrino, A. Petralia, V. Petrillo, L. Piersanti, M. A. Pocsai, K. Poder, R. Pompili, L. Pribyl, D. Pugacheva, B. A. Reagan, J. Resta-Lopez, R. Ricci, S. Romeo, M. Rossetti Conti, A. R. Rossi, R. Rossmanith, U. Rotundo, E. Roussel, L. Sabbatini, P. Santangelo, G. Sarri, L. Schaper, P. Scherkl, U. Schramm, C. B. Schroeder, J. Scifo, L. Serafini, G. Sharma, Z. M. Sheng, V. Shpakov, C. W. Siders, L. O. Silva, T. Silva, C. Simon, C. Simon-Boisson, U. Sinha, E. Sistrunk, A. Specka, T. M. Spinka, A. Stecchi, A. Stella, F. Stellato, M. J. V. Streeter, A. Sutherland, E. N. Svystun, D. Symes, C. Szwaj, G. E. Tauscher, D. Terzani, G. Toci, P. Tomassini, R. Torres, D. Ullmann, C. Vaccarezza, M. Valléau, M. Vannini, A. Vannozzi, S. Vescovi, J. M. Vieira, F. Villa, C. G. Wahlström, R. Walczak, P. A. Walker, K. Wang, A. Welsch, C. P. Welsch, S. M. Weng, S. M. Wiggins, J. Wolfenden, G. Xia, M. Yabashi, H. Zhang, Y. Zhao, J. Zhu, and A. Zigler. Eupraxia conceptual design report. *European Physical Journal: Special Topics*, 229:3675–4284, 2020. doi: https://doi.org/10.1140/epjst/e2020-000127-8.

90. T Poikela, J Plosila, T Westerlund, M Campbell, M De Gaspari, X Llopart, V Gromov, R Kluit, M van Beuzekom, F Zappon, V Zivkovic, C Brezina, K Desch, Y Fu, and A Kruth. Timepix3: a 65k channel hybrid pixel readout chip with simultaneous toa/tot and sparse readout. *Journal of Instrumentation*, 9(05):C05013, may 2014. doi: https://doi.org/10.1088/1748-0221/9/05/C05013.
91. R. Al Darwish, L. Marcu, and E. Bezak. Overview of current applications of the timepix detector in spectroscopy, radiation and medical physics. *Applied Spectroscopy Reviews*, 55(3):243–261, 2020. doi: https://doi.org/10.1080/05704928.2019.1580202.
92. K.A. Tanaka, K.M. Spohr, D.L. Balabanski, S. Balascuta, L. Capponi, M.O. Cernaianu, M. Cuciuc, A. Cucoanes, I. Dancus, A. Dhal, B. Diaconescu, D. Doria, P. Ghenuche, D.G. Ghita, S. Kisyov, V. Nastasa, J. F. Ong, F. Rotaru, D. Sangwan, P.-A. Söderström, D. Stutman, G. Suliman, O. Tesileanu, L. Tudor, N. Tsoneva, C.A. Ur, D. Ursescu, and N.V. Zamfir. Current status and highlights of the eli-np research program. *Matter and Radiation at Extremes*, 5(2):024402, 03 2020. doi: https://doi.org/10.1063/1.5093535.
93. A. Apyan, Mi.W. Krasny, and W. Płaczek. Gamma factory high-intensity muon and positron source: Exploratory studies. *Phys. Rev. Accel. Beams*, 26:083401, 2023. doi: https://doi.org/10.1103/PhysRevAccelBeams.26.083401.
94. A. Bălăceanu, M. Dobre, A. Gherghel-Lascu, A. Ilinca, M. Niculescu-Oglinzanu, A. Săftoiu, R.-I. Smău, D. Stanca, and C. Vancea. Characterization of the basic unit in a multi-channel sipm muography detector using cosmic muons. *Nuclear Instruments and Methods in Physics Research Section A: Accelerators, Spectrometers, Detectors and Associated Equipment*, 1051:168199, 2023. doi: https://doi.org/10.1016/j.nima.2023.168199.
95. C. Vancea, A. Bălăceanu, M. Dobre, A. Gherghel-Lascu, Mihai N.-O., A. Saftoiu, and Denis S. $\mu$ 36: a sipm-read scintillator detector designed for muography applications. *Journal of Instrumentation*, 20(05):P05019, 2025. doi: https://doi.org/10.1088/1748-0221/20/05/P05019.
96. A. Cimmino, V. Olšovcová, R. Versaci, D. Horváth, B. Lefebvre, A. Tsinganis, V. Stránský, R. Truneček, and Z. Trunečková. Radiation protection at petawatt laser-driven accelerator facilities: The eli beamlines case. *Nuclear Science and Engineering*, 198(2):245–263, 2024. doi: https://doi.org/10.1080/00295639.2023.2191585.
97. E. Sistrunk, T. Spinka, A. Bayramian, S. Betts, R. Bopp, S. Buck, K. Charron, J. Cupal, R. Deri,

Downloaded from https://www.cambridge.org/core. 19 Nov 2026 at 10:23:14, subject to the Cambridge Core terms of use.

M. Drouin, A. Erlandson, E. S. Fulkerson, J. Horner, J. Horacek, J. Jarboe, K. Kasl, D. Kim, E. Koh, L. Koubikova, R. Lanning, W. Maranville, C. Marshall, D. Mason, J. Menapace, P. Miller, P. Mazurek, A. Naylon, J. Novak, D. Peceli, P. Rosso, K. Schaffers, D. Smith, J. Stanley, R. Steele, S. Telford, J. Thoma, D. VanBlarcom, J. Weiss, P. Wegner, B. Rus, and C. Haefner. All diode-pumped, high-repetition-rate advanced petawatt laser system (hapls). In *Conference on Lasers and Electro-Optics*, page STh1L.2. Optica Publishing Group, 2017. doi: https://doi.org/10.1364/CLEO_SI.2017.STh1L.2.

98. G. Grittani, C. Lazzarini, S. Lorenz, M. Nevrkla, L. Vilanova, S. V. Bulanov, and G. Korn. Eli-elba: fundamental science investigations with high power lasers at eli-beamlines. In *OSA High-brightness Sources and Light-driven Interactions Congress 2020 (EUVXRAY, HILAS, MICS)*, page JM3A.20. Optica Publishing Group, 2020. doi: https://doi.org/10.1364/EUVXRAY.2020.JM3A.20.
99. S. Lorenz, G. Grittani, E. Chacon-Golcher, C. M. Lazzarini, J. Limpouch, F. Nawaz, M. Nevrkla, L. Vilanova, and T. Levato. Characterization of supersonic and subsonic gas targets for laser wakefield electron acceleration experiments. *Matter and Radiation at Extremes*, 4(1):015401, 01 2019. ISSN 2468-2047. doi: https://doi.org/10.1063/1.5081509.
100. S. Lorenz, G. Grittani, L. V. N. Goncalves, C. M. Lazzarini, J. Limpouch, M. Nevrkla, S. Bulanov, and G. Korn. Tomographic reconstruction algorithms for structured gas density profiles of the targets for laser wakefield acceleration. *Measurement Science and Technology*, 31(8):085205, may 2020. doi: https://doi.org/10.1088/1361-6501/ab7cf5.
101. F. Batysta, R. Antipenkov, T. Borger, A. Kissinger, J. T. Green, R. Kananavičius, G. Chériaux, D. Hidinger, J. Kolenda, E. Gaul, B. Rus, and T. Ditmire. Spectral pulse shaping of a 5 hz, multi-joule, broadband optical parametric chirped pulse amplification frontend for a 10 pw laser system. *Opt. Lett.*, 43(16):3866–3869, aug 2018. doi: https://doi.org/10.1364/OL.43.003866.
102. G. R. Lynch and O. I. Dahl. Approximations to multiple coulomb scattering. *Nuclear Instruments and Methods in Physics Research Section B: Beam Interactions with Materials and Atoms*, 58(1):6–10, 1991. doi: https://doi.org/10.1016/0168-583X(91)95671-Y.
103. G. Bonomi, P. Checchia, M. D'Errico, D. Pagano, and G. Saracino. Applications of cosmic-ray muons. *Progress in Particle and Nuclear Physics*, 112:103768, 2020. doi: https://doi.org/10.1016/j.ppnp.2020.103768.
104. K. N. Borozdin, G. E. Hogan, C. Morris, W. C. Priedhorsky, A. Saunders, L. J. Schultz, and M. E. Teasdale. Radiographic imaging with cosmic-ray muons. *Nature*, 422:277, 2003. doi: https://doi.org/10.1038/422277a.
105. V. Anghel, J. Armitage, F. Baig, K. Boniface, K. Boudjemline, J. Bueno, E. Charles, P-L. Drouin, A. Erlandson, G. Gallant, R. Gazit, D. Godin, V.V. Golovko, C. Howard, R. Hydomako, C. Jewett, G. Jonkmans, Z. Liu, A. Robichaud, T.J. Stocki, M. Thompson, and D. Waller. A plastic scintillator-based muon tomography system with an integrated muon spectrometer. *Nuclear Instruments and Methods in Physics Research Section A: Accelerators, Spectrometers, Detectors and Associated Equipment*, 798:12–23, 2015. doi: https://doi.org/10.1016/j.nima.2015.06.054.
106. J. Bae and S. Chatzidakis. The effect of cosmic ray muon momentum measurement for monitoring shielded special nuclear materials, 2022. URL https://arxiv.org/abs/2109.02470.
107. E. Guardincerri, J. Bacon, K. Borozdin, J. Matthew Durham, J. Fabritius II, A. Hecht, E. C. Milner, H. M., C. L. Morris, J. Perry, and D. Poulson. Detecting special nuclear material using muon-induced neutron emission. *Nuclear Instruments and Methods in Physics Research Section A: Accelerators, Spectrometers, Detectors and Associated Equipment*, 789:109–113, 2015. doi: https://doi.org/10.1016/j.nima.2015.03.070.
108. L. W. Alvarez, J. A. Anderson, F. El Bedwei, J. Burkhard, A. Fakhry, A. Girgis, A. Goneid, F. Hassan, D. Iverson, G. Lynch, Z. Miligy, A. H. Moussa, M. Sharkawi, and L. Yazolino. Search for hidden chambers in the pyramids. *Science*, 167(3919):832–839, 1970. doi: https://doi.org/10.1126/science.167.3919.832.
109. L. Cimmino, G. Baccani, P. Noli, L. Amato, F. Ambrosino, L. Bonechi, M. Bongi, V. Ciulli, R. D'Alessandro, M. D'Errico, S. Gonzi, B. Melon, G. Minin, G. Saracino, L. Scognamiglio, P. Strolin, and L. Viliani. 3d muography for the search of hidden cavities. *Sci Rep.*, 9(1):2974, 2019. doi: https://doi.org/10.1038/s41598-019-39682-5.
110. L. Gebhart and D. Snowden-Ifft. Muon tomography for detection of dynamic border tunnels. *Nuclear Instruments and Methods in Physics Research Section A: Accelerators, Spectrometers, Detectors and Associated Equipment*, 1053:168383, 2023. ISSN 0168-9002. doi: https://doi.org/10.1016/j.nima.2023.168383.
111. L. Oláh, H. K. M. Tanaka, and D. Varga, editors. *Muography: Exploring Earth's Subsurface with Elementary Particles*. American Geophysical Union (AGU), 2022. ISBN 9781119722748. doi: https://doi.org/10.1002/9781119722748.
112. G. Surányi, G. Molnár, G. G. Barnaföldi, G. Hamar, H. G. Melegh, L. Oláh, and D. Varga. Locating of density anomalies using highly-penetrating cosmic muons. *Szombathely*, 2016. doi: https://doi.org/10.17701/16.203-216.
113. I.L. Roche, S. Pasquet, K. Chalikakis, N. Mazzilli,

Downloaded from https://www.cambridge.org/core. 19 Nov 2026 at 10:23:14, subject to the Cambridge Core terms of use.

M. Rosas-Carbajal, J.-B. Decitre, L. Serene, C. Batiot-Guilhe, C. Emblanch, J. Marteau, and S. Gaffet. *Water Resource Management*, chapter 10, pages 137–152. American Geophysical Union (AGU), 2022. ISBN 9781119722748. doi: https://doi.org/10.1002/9781119722748.ch10.

114. J. Gluyas, L. Thompson, D. Allen, C. Benton, P. Chadwick, S. Clark, J. Klinger, V. Kudryavtsev, D. Lincoln, B. Maunder, C. Mitchell, S. Nolan, S. Paling, N. Spooner, L. Staykov, S. Telfer, D. Woodward, and M. Coleman. Passive, continuous monitoring of carbon dioxide geostorage using muon tomography. *Philosophical Transactions of The Royal Society A Mathematical Physical and Engineering Sciences*, 377: 20180059, 2018. doi: https://doi.org/10.1098/rsta.2018.0059.
115. K. Morishima, M. Kuno, A. Nishio, N. Kitagawa, Y. Manabe, M. Moto, F. Takasaki, H. Fujii, K. Satoh, H. Kodama, K. Hayashi, S. Odaka, S. Procureur, D. Attié, S. Bouteille, D. Calvet, C. Filosa, P. Magnier, I. Mandjavidze, M. Riallot, B. Marini, P. Gable, Y. Date, M. Sugiura, Y. Elshayeb, T. Elnady, M. Ezzy, E. Guerriero, V. Steiger, N. Serikoff, J.-B. Mouret, B. Charlès, H. Helal, and M. Tayoubi. Discovery of a big void in khufu's pyramid by observation of cosmic-ray muons. *Nature*, 552:386–390, 2017. doi: https://doi.org/10.1038/nature24647.
116. S. Aguilar, R. Alfaro, E. Belmont, R. Cadena, V. Grabski, T. Ibarra, V. Lemus, L. R. Manzanilla, A. Martínez-Dávalos, A. Menchaca-Rocha, M. Moreno, and A. Sandoval. Search for cavities in the teotihuacan pyramid of the sun using cosmic muons: preliminary results. In *Proc. 33rd ICRC*, volume 4, pages 325–328, 2013. doi: https://doi.org/10.7529/ICRC2011/V04/1117.
117. G. Liu, X. Luo, H. Tian, K. Yao, F. Niu, L. Jin, J. Gao, J. Rong, Z. Fu, Y. Kang, Y. Fu, C. Wu, H. Gao, J. Gong, W. Zhang, X. Luo, C. Liu, X. Tian, M. Yu, F. Wu, J. Chen, J. Liu, and Z. Liu. High-precision muography in archaeogeophysics: A case study on xi'an defensive walls. *Journal of Applied Physics*, 133(1):014901, 01 2023. doi: https://doi.org/10.1063/5.0123337.
118. D. Borselli, T. Beni, L. Bonechi, M. Bongi, R. Ciaranfi, V. Ciulli, R. D'Alessandro, L. Fanò, C. Frosin, S. Gonzi, L. Lombardi, L. Melelli, A. Paccagnella, and M. Turchetti. Muographic study of the palazzone necropolis (perugia-italy). *Journal of Advanced Instrumentation in Science*, 2024, 01 2024. doi: https://doi.org/10.31526/JAIS.2024.467.
119. J. Marteau, J. de Bremond d'Ars, D. Gibert, K. Jourde, J.-C. Ianigro, and B. Carlus. Diaphane: muon tomography applied to volcanoes, civil engineering, archaelogy. *Journal of Instrumentation*, 12:C02008, 2017. doi: https://doi.org/10.1088/1748-0221/12/02/C02008.
120. A. Zenoni, G. Bonomi, A. Donzella, M. Subieta, G. Baronio, I. Bodini, D. Cambiaghi, M. Lancini, D. Vetturi, O. Barnabà, F. Fallavollita, R. Nardò, C. Riccardi, M. Rossella, P. Vitulo, and G. Zumerle. Historical building stability monitoring by means of a cosmic ray tracking system, 2014. URL https://arxiv.org/abs/1403.1709.
121. A. Giammanco, M. Al Moussawi, M. Boone, T. De Kock, J. De Roy, S. Huysmans, V. Kumar, M. Lagrangev, and M. Tytgat. Toward using cosmic rays to image cultural heritage objects. *iScience*, 28(3):112094, 2025. doi: https://doi.org/10.1016/j.isci.2025.112094.
122. S. Miyamoto, S. Nagahara, K. Morishima, T. Nakano, M. Koyama, and Y. Suzuki. A muographic study of a scoria cone from 11 directions using nuclear emulsion cloud chambers. *Geoscientific Instrumentation, Methods and Data Systems*, 11(1):127–147, 2022. doi: https://doi.org/10.5194/gi-11-127-2022.
123. D.P. Aguillard, T. Albahri, D. Allspach, A. Anisenkov, K. Badgley, S. Baeßler, I. Bailey, L. Bailey, V.A. Baranov, E. Barlas-Yucel, T. Barrett, E. Barzi, F. Bedeschi, M. Berz, M. Bhattacharya, H.P. Binney, P. Bloom, J. Bono, E. Bottalico, T. Bowcock, S. Braun, M. Bressler, G. Cantatore, R.M. Carey, B.C.K. Casey, D. Cauz, R. Chakraborty, A. Chapelain, S. Chappa, S. Charity, C. Chen, M. Cheng, R. Chislett, Z. Chu, T.E. Chupp, C. Claessens, M. E. Convery, S. Corrodi, L. Cotrozzi, J. D. Crnkovic, S. Dabagov, P.T. Debevec, S. Di Falco, G. Di Sciascio, B. Drendel, A. Driutti, V.N. Duginov, M. Eads, A. Edmonds, J. Esquivel, M. Farooq, R. Fatemi, C. Ferrari, M. Fertl, A.T. Fienberg, A. Fioretti, D. Flay, S. B. Foster, H. Friedsam, N.S. Froemming, C. Gabbanini, I. Gaines, M.D. Galati, S. Ganguly, A. Garcia, J. George, L.K. Gibbons, A. Gioiosa, K.L. Giovanetti, P. Girotti, W. Gohn, L. Goodenough, T. Gorringe, J. Grange, S. Grant, F. Gray, S. Haciomeroglu, T. Halewood-Leagas, D. Hampai, F. Han, J. Hempstead, D. W. Hertzog, G. Hesketh, E. Hess, A. Hibbert, Z. Hodge, K. W. Hong, R. Hong, T. Hu, Y. Hu, M. Iacovacci, M. Incagli, P. Kammel, M. Kargiantoulakis, M. Karuza, J. Kaspar, D. Kawall, L. Kelton, A. Keshavarzi, D. S. Kessler, K.S. Khaw, Z. Khechadoorian, N.V. Khomutov, B. Kiburg, M. Kiburg, O. Kim, N. Kinnaird, E. Kraegeloh, V.A. Krylov, N.A. Kuchinskiy, K.R. Labe, J. LaBounty, M. Lancaster, S. Lee, B. Li, D. Li, L. Li, I. Logashenko, A. Lorente Campos, Z. Lu, A. Lucà, G. Lukicov, A. Lusiani, A.L. Lyon, B. MacCoy, R. Madrak, K. Makino, S. Mastroianni, J. P. Miller, S. Miozzi, B. Mitra, J.P. Morgan, W.M. Morse, J. Mott, A. Nath, J.K. Ng, H. Nguyen, Y. Oksuzian, Z. Omarov, R. Osofsky, S. Park, G. Pauletta, G. M. Piacentino, R. N. Pilato, K.T. Pitts, B. Plaster, D. Počanić, N. Pohlman, C.C. Polly, J. Price, B. Quinn, M.U H. Qureshi, S. Ramachandran, E. Ramberg, R. Reimann, B. L. Roberts, D.L. Rubin, L. Santi, C. Schlesier, A. Schreckenberger, Y. K.

Downloaded from https://www.cambridge.org/core. 19 Nov 2026 at 10:23:14, subject to the Cambridge Core terms of use.

Semertzidis, D. Shemyakin, M. Sorbara, D. Stöckinger, J. Stapleton, D. Still, C. Stoughton, D. Stratakis, H.E. Swanson, G. Sweetmore, D.A. Sweigart, M.J. Syphers, D.A. Tarazona, T. Teubner, A.E. Tewsley-Booth, V. Tishchenko, N.H. Tran, W. Turner, E. Valetov, D. Vasilkova, G. Venanzoni, V.P. Volnykh, T. Walton, A. Weisskopf, L. Welty-Rieger, P. Winter, Y. Wu, B. Yu, M. Yucel, Y. Zeng, and C. Zhang. Measurement of the positive muon anomalous magnetic moment to 0.20 ppm. *Phys. Rev. Lett.*, 131:161802 – 161807, 2023. doi: https://doi.org/10.1103/PhysRevLett.131.161802.

124. M. Aoki, A. M. Baldini, R. H. Bernstein, C. Carloganu, S. Mihara, S. Miscetti, T. Mori, W. Ootani, F. Renga, S. Ritt, and A. Schoening. Charged lepton flavour violations searches with muons: present and future, 2025.
125. P. Crivelli. The mu-mass (muonium laser spectroscopy) experiment. *Hyperfine Interactions*, 239, 11 2018. doi: https://doi.org/10.1007/s10751-018-1525-z.
126. K.R. Long, D. Lucchesi, M.A. Palmer, N. Pastrone, D. Schulte, and V. Shiltsev. Muon colliders to expand frontiers of particle physics. *Nat. Phys.*, 17:289–292, 2021. doi: https://doi.org/10.1038/s41567-020-01130-x.
127. Y. Hamada, R. Kitano, R. Matsudo, H. Takaura, and M. Yoshida. tristan. *Progress of Theoretical and Experimental Physics*, 2022(5):053B02, 03 2022. doi: https://doi.org/10.1093/ptep/ptac059.
128. The ATLAS Collaboration. Observation of a new particle in the search for the standard model higgs boson with the atlas detector at the lhc. *Physics Letters B*, 716(1): 1–29, 2012. doi: https://doi.org/10.1016/j.physletb.2012.08.020.
129. The CMS Collaboration. Observation of a new boson at a mass of 125 gev with the cms experiment at the lhc. *Physics Letters B*, 716(1):30–61, 2012. doi: https://doi.org/10.1016/j.physletb.2012.08.021.
130. S. Eliezer. Muon catalyzed nuclear fusion. *Laser and Particle Beams*, 6(1):63–81, 1988. doi: https://doi.org/10.1017/S0263034600003815.
131. S. Eliezer and Z. Henis. Muon-catalyzed fusion-an energy production perspective. *Fusion Technology*, 26(1), 08 1994. ISSN ISSN 0748-1896. URL https://www.osti.gov/biblio/105359.
132. J.D. Jackson. Catalysis of nuclear reactions between hydrogen isotopes by $\mu^-$ mesons. *Phys. Rev.*, 106:330–339, 1957. doi: https://doi.org/10.1103/PhysRev.106.330.
133. J.-L. Basdevant. *The Hydrogen Atom*, pages 251–274. Springer International Publishing, Cham, 2023. ISBN 978-3-031-17635-7. doi: https://doi.org/10.1007/978-3-031-17635-7_12.
134. S.D. Moustaizis, P. Lalousis, H. Hora, Z. Henis, S. Eliezer, and I. Ploumistakis. New scheme to trigger fusion in a compact magnetic fusion device by combining muon catalysis and alpha heating effects. *High Power Laser Science and Engineering*, 4:e42, 2016. doi: https://doi.org/10.1017/hpl.2016.41.
135. C. Daponta, S. Moustaizis, S. Eliezer, Z. Henis, P. Lalousis, N. Nissim, and Y. Schweitzer. Towards p-11B medium configurations with high $P_{fus}/P_{Brems}$ ratios. *Frontiers in Physics*, 12, 2024. doi: https://doi.org/10.3389/fphy.2024.1425963.
136. T. Ditmire, J. Zweiback, V. Yanovsky, T. E. Cowan, G. Hays, and K.B. Wharton. Nuclear fusion from explosions of femtosecond laser-heated deuterium clusters. *Nature*, 398:489–492, 1999. doi: https://doi.org/10.1038/19037.
137. G. Grillon, Ph. Balcou, J.-P. Chambaret, D. Hulin, J. Martino, S. Moustaizis, L. Notebaert, M. Pittman, Th. Pussieux, A. Rousse, J-Ph. Rousseau, S. Sebban, O. Sublemontier, and M. Schmidt. Deuterium-deuterium fusion dynamics in low-density molecular-cluster jets irradiated by intense ultrafast laser pulses. *Phys. Rev. Lett.*, 89:065005, 2002. doi: https://doi.org/10.1103/PhysRevLett.89.065005.
138. I.C.E. Turcu, D. Margarone, L. Giuffrida, A. Picciotto, C. Spindloe, A.P.L. Robinson, and D. Batani. Borane (BmHn), hydrogen rich, proton boron fusion fuel materials for high yield laser-driven alpha sources. *Journal of Instrumentation*, 19(03):C03065, 2024. doi: https://doi.org/10.1088/1748-0221/19/03/C03065.
139. A. Picciotto, M. Valt, D.P. Molloy, A. Gaiardo, A. Milani, V. Kantarelou, L. Giuffrida, G. Nersisyan, A. McNamee, J.P. Kennedy, C.R.J. Fitzpatrick, P. Martin, D. Orecchia, A. Maffini, P. Scauso, L. Vanzetti, I.C.E. Turcu, L. Ferrario, R. Hall-Wilton, and D. Margarone. Ammonia borane-based targets for new developments in laser-driven proton boron fusion. *Applied Surface Science*, 672:160797, 2024. doi: https://doi.org/10.1016/j.apsusc.2024.160797.
140. P. Tchórz, T. Chodukowski, M. Rosiński, S. Borodziuk, M. Szymański, R. Dudžák, S. Singh, M. Krupka, T. Burian, A. Marchenko, M. Kustosz, and S. Agarwal. Proton beams generated via thermonuclear deuterium–deuterium fusion by means of modified cavity pressure acceleration-type targets as a candidate for proton–boron fusion driver. *Physics of Plasmas*, 31(8): 084503, 2024. doi: https://doi.org/10.1063/5.0207108.
141. L. Kiani, T. Zhou, S.-W. Bahk, J. Bromage, D. Bruhwiler, E.M. Campbell, Z. Chang, E. Chowdhury, M. Downer, and Q. Du. High average power ultrafast laser technologies for driving future advanced accelerators. *Journal of Instrumentation*, 18:T08006, 2023. doi: https://doi.org/10.1063/5.0207108.
142. Y. Wang, H. Chi, C. Baumgarten, K. Dehne, A.R. Meadows, A. Davenport, G. Murray, B.A. Reagan, C.S. Menoni, and J.J. Rocca. 1.1j yb:yag picosecond laser at 1khz repetition rate. *Optics Letters*, 2020. doi: https://doi.org/10.1364/OL.413129.

Downloaded from https://www.cambridge.org/core. 19 Nov 2026 at 10:23:14, subject to the Cambridge Core terms of use.